AD-A173 355 PERFORMANCE OF MISMATCHED RECEIVERS AGAINST RANGE SPREAD SCATTERERS(U) NAVAL UNDERWATER SYSTEMS CENTER NEWPORT RI W S HAUCK 19 SEP 86 NUSC-TR-7779 1/2

UNCLASSIFIED F/G 9/4 NL

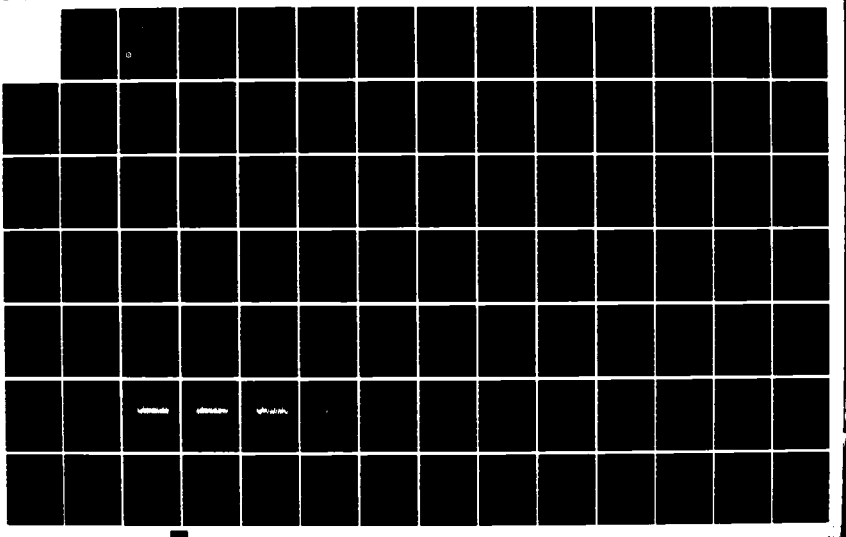

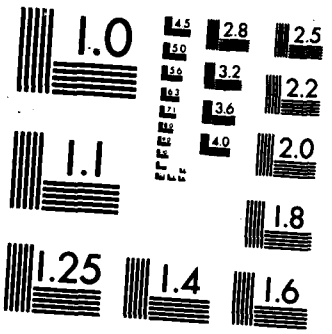

MICROCOPY RESOLUTION TEST CHART
NATIONAL BUREAU OF STANDARDS-1963-A

NUSC Technical Report 7779
19 September 1986

Performance of Mismatched Receivers Against Range Spread Scatterers

Walter S. Hauck III
Surface Ship Sonar Department

Naval Underwater Systems Center
Newport, Rhode Island / New London, Connecticut

Approved for public release; distribution unlimited.

Preface

This report was prepared as a thesis in partial fulfillment of the requirements for the degree Master of Science in Acoustics at the Pennsylvania State University.

Support for this report was provided under NUSC Project No. A65000, EVA Support for Shipboard Sonar, Principal Investigator, P. D. Herstein, Code 33A3. Funding was provided under Program Element No. 62759 through the Naval Research Laboratory, L. Bruce Palmer, Acting Program Manager, EVA Support for Shipboard Sonar.

The author would like to thank the thesis committee members, Dr. Carter Ackerman, Dr. Dennis Ricker and Dr. Alan Stuart for several discussions and diligent comments concerning this work. I am particularly grateful to Drs. Ackerman and Ricker for their continuing support over a number of years, which allowed the thesis to be successfully completed. I would also like to thank the following people at the Naval Underwater Systems Center, New London, Connecticut, for their vigorous support, assistance and review of early drafts: Peter Herstein, Bernard Cole, Dr. Albert Nuttall, Dr. John Ianniello and Dr. William Roderick, Richard Vogelsong, and David Bostian.

Reviewed and Approved: 19 September 1986

L. Freeman
Head, Surface Ship Sonar Department

W. A. Von Winkle
Associate Technical Director
for Technology

UNCLASSIFIED
SECURITY CLASSIFICATION OF THIS PAGE

ADA173355

REPORT DOCUMENTATION PAGE

1a. REPORT SECURITY CLASSIFICATION UNCLASSIFIED	1b. RESTRICTIVE MARKINGS
2a. SECURITY CLASSIFICATION AUTHORITY	3. DISTRIBUTION/AVAILABILITY OF REPORT Approved for public release; distribution unlimited.
2b. DECLASSIFICATION/DOWNGRADING SCHEDULE	
4. PERFORMING ORGANIZATION REPORT NUMBER(S) TR 7779	5. MONITORING ORGANIZATION REPORT NUMBER(S)
6a. NAME OF PERFORMING ORGANIZATION Naval Underwater Systems Center 6b. OFFICE SYMBOL (If applicable)	7a. NAME OF MONITORING ORGANIZATION
6c. ADDRESS (City, State, and ZIP Code) New London Laboratory New London, CT 06320	7b. ADDRESS (City, State, and ZIP Code)
8a. NAME OF FUNDING/SPONSORING ORGANIZATION Naval Research Laboratory 8b. OFFICE SYMBOL (If applicable)	9. PROCUREMENT INSTRUMENT IDENTIFICATION NUMBER
8c. ADDRESS (City, State, and ZIP Code) Washington, D. C. 20375	10. SOURCE OF FUNDING NUMBERS PROGRAM ELEMENT NO. / PROJECT NO. / TASK NO. / WORK UNIT ACCESSION NO.

11. TITLE (Include Security Classification)
PERFORMANCE OF MISMATCHED RECEIVERS AGAINST RANGE SPREAD SCATTERERS

12. PERSONAL AUTHOR(S)
Walter S. Hauck III

13a. TYPE OF REPORT	13b. TIME COVERED FROM ____ TO ____	14. DATE OF REPORT (Year, Month, Day)	15. PAGE COUNT
		1986 September 19	

16. SUPPLEMENTARY NOTATION

17. COSATI CODES			18. SUBJECT TERMS (Continue on reverse if necessary and identify by block number)
FIELD	GROUP	SUB-GROUP	Scattering Function Ambiguity Function Correlation Receiver Performance Prediction

19. ABSTRACT (Continue on reverse if necessary and identify by block number)

This report examines the output signal-to-noise ratio of a complex correlation receiver for signals scattered from three types of range spread scattering functions: 1) the continuous scatterer, 2) the slowly fluctuating point scatterer, and 3) the composite scatterer, a scatterer with both a continuous scattering component and two point scatterers at fixed positions along the continuous scatterer. The matched filter receiver has an integration time equal to the transmit signal length. However in the case of range or time spreading, this receiver is suboptimum. Increasing the receiver integration time beyond the length of the transmit pulse increases the receiver performance measured in terms of signal-to-noise. The output signal-to-noise ratio may be predicted analytically using simple scattering functions and transmit and receiver processing waveforms. This prediction is compared to simulated performance for fourteen combinations of scattering strength, and noise parameters are examined.

20. DISTRIBUTION/AVAILABILITY OF ABSTRACT	21. ABSTRACT SECURITY CLASSIFICATION
☒ UNCLASSIFIED/UNLIMITED ☐ SAME AS RPT. ☐ OTIC USERS	UNCLASSIFIED
22a. NAME OF RESPONSIBLE INDIVIDUAL Walter S. Hauck III	22b. TELEPHONE (Include Area Code) (203) 440-6000 / 22c. OFFICE SYMBOL Code 3331

DD FORM 1473, 84 MAR 83 APR edition may be used until exhausted. All other editions are obsolete.

SECURITY CLASSIFICATION OF THIS PAGE
UNCLASSIFIED

19. (CONT'D.)

In addition, the effects of correlated continuous scatter are discussed. By filtering the continuous scatterer to produce correlated scatter, the output of the receiver is increased relative to the uncorrelated scattering prediction. The increase in signal-to-noise ratio is inversely related to the bandwidth of the filter. Comparisons are made for three sets of scattering strength parameters and four filter bandwidths.

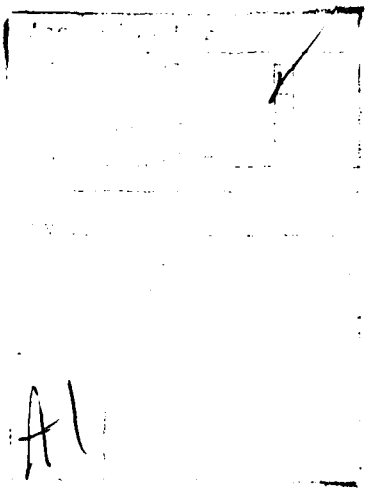

TABLE OF CONTENTS

Page

LIST OF TABLES iii

LIST OF FIGURES iv

LIST OF SYMBOLS ix

Chapter

1. INTRODUCTION 1

2. MODEL ANALYSIS USING SCATTERING AND AMBIGUITY FUNCTIONS 7
   - 2.1 Introduction 7
   - 2.2 Complex Envelopes and Narrowband Signals . . . 7
   - 2.3 The Range Scattering Function 8
     - 2.3.1 Definition 8
     - 2.3.2 Composite Scattering Function 11
   - 2.4 Receiver Ambiguity Function 12
     - 2.4.1 Receiver Model 12
     - 2.4.2 Receiver Ambiguity Function 14

3. SIMULATION OF SCATTERER AND RECEIVER MODELS 17
   - 3.1 Simulation of Composite Scattering Function . 17
     - 3.1.1 Simulation of a Continuous Scatterer . 17
     - 3.1.2 Simulation of Point Scatterers 18
   - 3.2 Generation of Simulated and Predicted SNR . . 19
     - 3.2.1 Simulation of Reflected Signal 19
     - 3.2.2 Generation of Simulated and Predicted SNR 20

4. COMPARISON OF PREDICTED AND SIMULATED SNR 25
   - 4.1 Introduction 25
     - 4.1.1 Introduction 25
     - 4.1.2 Calculation of Comparison Data 27
     - 4.1.3 Presentation of Comparison Data . . . 28
   - 4.2 The Continuous Scatterer in Noise 30
     - 4.2.1 Continuous Scatterer in Noise 30
     - 4.2.2 Distribution of Simulated SNR 32
     - 4.2.3 Comparison as a Function of SNR . . . 33
   - 4.3 Point Reflectors in Noise 36
   - 4.4 The Composite Scatterer in Noise 38
     - 4.4.1 Composite Scatterer in Noise 38
     - 4.4.2 Effects of Simulation Sample Size . . 47

TABLE OF CONTENTS (Cont'd)

	Page
5. RECEIVER PERFORMANCE FOR CORRELATED CONTINUOUS SCATTER	
5.1 Modifications to VanTrees' Model	52
5.1.1 Introduction	52
5.1.2 Simulation of the Correlated Continuous Scatterer	52
5.2 Correlated Continuous Scatterer Results	61
5.2.1 SNR Comparison versus Bandwidth	61
5.2.2 Corrections for Correlated Scattering	69
5.3 Composite Correlated Scatterer SNR Comparison	72
6. CONCLUSIONS	83
6.1 Summary and Conclusions	83
6.1.1 Models	83
6.1.2 Simulation	84
6.1.3 Results and Errors	84
6.1.4 Correlated Scattering	86
6.2 Recommendations for Further Study	87
ANNOTATED BIBLIOGRAPHY	89
APPENDIX A: DERIVATION OF THE CROSSAMBIGUITY FUNCTION	91
APPENDIX B: GENERATION OF RANDOM NUMBERS	94
B.1 Generation of Uniform Random Numbers	94
B.2 Generation of Gaussian Numbers	94
APPENDIX C: CALCULATION OF THE VARIANCE OF SIGNAL-TO-NOISE RATIO	101

LIST OF TABLES

Table		Page
1.	Constant Simulation Scattering and Receiver Model Parameters	21
2.	Scattering Strength Parameters and Statistics of Differences between Simulated and Predicted Signal-to-Noise Ratios for 14 Combinations of Scattering Strength Parameters	26
3.	Scattering Strength Parameters and Statistics of Differences between Simulated and Predicted Signal-to-Noise Ratios Assuming Correlated Continuous Scattering Combinations of Scattering Strength	62
4.	Coefficients of Polynomials Fitted to Continuous Correlated Scatterer Gain versus Filter Bandwidth Data (see Figure 35)	71

LIST OF FIGURES

Figure		Page
1.	Block diagram of complex crosscorrelation receiver	5
2.	Magnitude of the composite scattering function (top), and reflected signal (bottom). Note the difference between the time axes	13
3.	Comparison of predicted and simulated SNR for Case 1; $\sigma_{CS} = 1$, $\sigma_{HI} = 0$, $\sigma_N = 1$. Predicted values are shown as circles, simulated data shown as squares . .	29
4.	Comparison of normalized SNR for Case 1; $\sigma_{CS} = 1$, $\sigma_{HI} = 0$, $\sigma_N = 1$. Predicted values are shown as circles, simulated data shown as squares	31
5.	Comparison of predicted and simulated SNR for Case 11; $\sigma_{CS} = 1$, $\sigma_{HI} = 0$, $\sigma_N = 1000$. Predicted values are shown as circles, simulated data shown as squares . .	34
6.	Comparison of normalized SNR for Case 11; $\sigma_{CS} = 1$, $\sigma_{HI} = 0$, $\sigma_N = 1000$. Predicted values are shown as circles, simulated data shown as squares	35
7.	Comparison of predicted and simulated SNR for Case 2; $\sigma_{CS} = 0$, $\sigma_{HI} = 1$, $\sigma_N = 1$. Predicted values are shown as circles, simulated data shown as squares . .	37
8.	Comparison of normalized SNR for Case 2; $\sigma_{CS} = 0$, $\sigma_{HI} = 1$, $\sigma_N = 1$. Predicted values are shown as circles, simulated data shown as squares	39
9.	Comparison of predicted and simulated SNR for Case 6; $\sigma_{CS} = 0$, $\sigma_{HI} = 1$, $\sigma_N = 100$. Predicted values are shown as circles, simulated data shown as squares . .	40
10.	Comparison of normalized SNR for Case 6; $\sigma_{CS} = 0$, $\sigma_{HI} = 1$, $\sigma_N = 100$. Predicted values are shown as circles, simulated data shown as squares	41
11.	One realization of the signal reflected from the composite scatterer for large point scatterer reflectivity	42

LIST OF FIGURES (Cont'd)

Figure		Page
12.	Comparison of predicted and simulated SNR for Case 8; $\sigma_{CS} = 1$, $\sigma_{HI} = 100$, $\sigma_N = 1$. Predicted values are shown as circles, simulated data shown as squares . .	44
13.	Comparison of normalized SNR for Case 8; $\sigma_{CS} = 1$, $\sigma_{HI} = 100$, $\sigma_N = 1$. Predicted values are shown as circles, simulated data shown as squares	45
14.	Comparison of predicted and simulated SNR for Case 7; $\sigma_{CS} = 1$, $\sigma_{HI} = 10$, $\sigma_N = 1$. Predicted values are shown as circles, simulated data shown as squares . .	46
15.	Comparison of normalized SNR for Case 7; $\sigma_{CS} = 1$, $\sigma_{HI} = 10$, $\sigma_N = 1$. Predicted values are shown as circles, simulated data shown as squares	48
16.	Comparison of predicted and simulated SNR for Case 8; $\sigma_{CS} = 1$, $\sigma_{HI} = 100$, $\sigma_N = 1$. Simulated SNR values obtained by averaging 1000 realizations of the scattering function. Predicted values are shown as circles, simulated data shown as squares	49
17.	Comparison of normalized SNR for Case 8; $\sigma_{CS} = 1$, $\sigma_{HI} = 100$, $\sigma_N = 1$. Simulated SNR values obtained by averaging 1000 realizations of the scattering function. Predicted values are shown as circles, simulated data shown as squares	51
18.	Frequency response of filter used to generate the correlated scattering sequence. The filter bandwidth is 0.49	54
19.	Frequency response of filter used to generate the correlated scattering sequence. The filter bandwidth is 0.01	55
20.	Uncorrelated scattering sequence. Sequence energy = 65.95 dB	59
21.	Correlated scattering sequence for a filter bandwidth of 0.49. Sequence energy = 65.95 dB	57
22.	Correlated scattering sequence for a filter bandwidth of 0.25. Sequence energy = 65.95 dB	58

LIST OF FIGURES (Cont'd)

Figure		Page
23.	Correlated scattering sequence for a filter bandwidth of 0.1. Sequence energy = 65.95 dB	59
24.	Correlated scattering sequence for a filter bandwidth of 0.01. Sequence energy = 65.95 dB	60
25.	Comparison of uncorrelated continuous scattering SNR prediction, and correlated scattering simulation for Case 15; $\sigma_{CS} = 1$, $\sigma_{HI} = 0$, $\sigma_N = 1$, filter bandwidth = 0.49. Predicted values are shown as circles, simulated data shown as squares	63
26.	Comparison of normalized uncorrelated continuous scattering SNR prediction, and correlated scattering simulation for Case 15; $\sigma_{CS} = 1$, $\sigma_{HI} = 0$, $\sigma_N = 1$, filter bandwidth = 0.49. Predicted values are shown as circles, simulated data shown as squares	64
27.	Comparison of uncorrelated continuous scattering SNR prediction, and correlated scattering simulation for Case 16; $\sigma_{CS} = 1$, $\sigma_{HI} = 0$, $\sigma_N = 1$, filter bandwidth = 0.25. Predicted values are shown as circles, simulated data shown as squares	65
28.	Comparison of uncorrelated continuous scattering SNR prediction, and correlated scattering simulation for Case 17; $\sigma_{CS} = 1$, $\sigma_{HI} = 0$, $\sigma_N = 1$, filter bandwidth = 0.1. Predicted values are shown as circles, simulated data shown as squares	66
29.	Comparison of uncorrelated continuous scattering SNR prediction, and correlated scattering simulation for Case 18; $\sigma_{CS} = 1$, $\sigma_{HI} = 0$, $\sigma_N = 1$, filter bandwidth = 0.01. Predicted values are shown as circles, simulated data shown as squares	67
30.	Exponential fit to SNR gain versus filter bandwidth for $\alpha = 5.6$, 5.8 and 5.9. SNR gain obtained from simulation is shown as the solid line	70
31.	Polynomial fit to SNR gain versus filter bandwidth for polynomial orders, N, = 2, 3 and 4. SNR gain obtained from simulation is shown as the solid line	73

LIST OF FIGURES (Cont'd)

Figure		Page
32.	Best fits for polynomial and exponential models to SNR gain versus filter bandwidth. SNR gain otbained from simulation is shown as the solid line	74
33.	Comparison of uncorrelated continuous scattering SNR prediction, and correlated scattering simulation for Case 19; $\sigma_{CS} = 1$, $\sigma_{HI} = 100$, $\sigma_N = 1$, filter bandwidth = 0.49. Predicted values are shown as circles, simulated data shown as squares	75
34.	Comparison of normalized uncorrelated continuous scattering SNR prediction, and correlated scattering simulation for Case 19; $\sigma_{CS} = 1$, $\sigma_{HI} = 100$, $\sigma_N = 1$, filter bandwidth = 0.49. Predicted values are shown as circles, simulated data shown as squares	76
35.	Comparison of uncorrelated continuous scattering SNR prediction, and correlated scattering simulation for Case 20; $\sigma_{CS} = 1$, $\sigma_{HI} = 100$, $\sigma_N = 1$, filter bandwidth = 0.25. Predicted values are shown as circles, simulated data shown as squares	77
36.	Comparison of normalized uncorrelated continuous scattering SNR prediction, and correlated scattering simulation for Case 20; $\sigma_{CS} = 1$, $\sigma_{HI} = 100$, $\sigma_N = 1$, filter bandwidth = 0.25. Predicted values are shown as circles, simulated data shown as squares	78
37.	Comparison of uncorrelated continuous scattering SNR prediction, and correlated scattering simulation for Case 21; $\sigma_{CS} = 1$, $\sigma_{HI} = 100$, $\sigma_N = 1$, filter bandwidth = 0.10. Predicted values are shown as circles, simulated data shown as squares	79
38.	Comparison of uncorrelated continuous scattering SNR prediction, and correlated scattering simulation for Case 22; $\sigma_{CS} = 1$, $\sigma_{HI} = 100$, $\sigma_N = 1$, filter bandwidth = 0.01. Predicted values are shown as circles, simulated data shown as squares	80
39.	Histogram of random number generator for a sample set size of 100. Distribution mean = 0.04, and standard deviation = 0.92	96

LIST OF FIGURES (Cont'd)

Figure		Page
40.	Histogram of random number generator for a sample set size of 1000. Distribution mean = 0.1, and standard deviation = 1.01	97
41.	Autocorrelation of random number generator output for a sample set size of 1024	98
42.	Crosscorrelation of random number generator output for a sample set size of 1024	100

LIST OF SYMBOLS

α	SNR gain factor
$\Gamma(x)$	Gamma function
ρ_E	Continuous energy scattering density
σ_{cs}^2	Variance of continuous scatterer
σ_{Data}^2	Variance of difference between predicted and simulated SNR
σ_{Edge}^2	Variance of reflected signal onset
σ_{HI}^2	Variance of point scatterers
σ_N^2	Variance of noise
τ	Actual time delay
τ'	$\tau - \tau_0$
τ_i	Delay of $i^{\underline{th}}$ point scatterer
$\Delta\tau_i$	Delay of signal reflected from $i^{\underline{th}}$ range increment
τ_0	Hypothesized time delay
$\chi(\tau,\omega)$	Delay-Doppler crosscorrelation function
$\left\|\chi(\tau,\omega)\right\|^2$	Crossambiguity Function
ω	Doppler
ω'	$\omega - \omega_0$
ω_c	Radian carrier frequency
ω_0	Hypothesized carrier frequency

$A_0 \ldots A_n$	Polynomial coefficients
$A(\tau',\omega')$	Autoambiguity function
$\tilde{b}$	Gaussian random variable
$B(x,y)$	Beta function
BW	Normalized filter bandwidth
c	Speed of sound
$E\{\ \}$	Expected value
$\bar{E}$	Geometric average difference between predicted and simulated SNR
E_i	Reflectivity of $i^{\underline{th}}$ point scatterer
E_n	Received noise energy
E_r	Received signal energy
E_T	Transmit signal energy
$F(n,m)$	F distribution
$f(t)$	Transmit waveform
f_s	Sampling frequency
$g(t)$	Receiver processing waveform
j	$\sqrt{-1}$
J,k	Number of averaged receiver outputs
$K(\tau,\tau_1)$	Covariance of $b(\tau)$ and $b(\tau_1)$
$K_s(t,t_1)$	Covariance of $s(t)$ and $s(t_1)$
ΔL_i	$i^{\underline{th}}$ Range increment
M	Sample index
N	Polynomial degree
NFFT	Integer FFT size
$\lvert N_k \rvert^2$	$k^{\underline{th}}$ Received noise energy

N_0	Noise power spectral density
NT	Number of samples in received signal
NTAR	Number of samples in continuous scatterer
NT_s	Number of samples in transmit signal
$P_X(u)$	Probability density function
r	Variance ratio
$\tilde{r}(n)$	Complex Gaussian process
$\tilde{r}_I(n)$	Imaginary part of $\tilde{r}(n)$
$\tilde{r}_R(n)$	Real part of $\tilde{r}(n)$
r(t)	Received signal
s(t)	Narrowband signal
$\tilde{s}(t)$	Complex envelope of s(t)
$S(\tau,\omega)$	Scattering function
$S_{CS}(\tau)$	Continuous range spread scattering function
$S_{HI}(\tau)$	Point scattering function
sinc(x)	sin(x)/x function
$\|S_k\|^2$	$k^{\underline{th}}$ Signal energy
$S_R(\tau)$	Range spread scattering function
SNR	Signal-to-Noise Ratio
T	Receiver integration time
T_s	Transmit pulse length
T_T	Duration of continuous scattered signal
u^Θ	$\Theta^{\underline{th}}$ Moment

CHAPTER 1

INTRODUCTION

In this thesis a comparison of simulated and predicted performance of a complex crosscorrelation receiver against a range spread scatterer is discussed. Performance is measured by the ratio of the receiver output signal energy to receiver output for noise only. This ratio can be predicted assuming analytic expressions for a singly spread target scattering function and the transmit and receiver waveforms. The signal-to-noise ratio, at the output of the receiver SNR, is examined as a function of receiver integration time, for a fixed input SNR. The prediction equation was developed by Ricker, and is derived in terms of the range spread function and the receiver crossambiguity function [1]. The simulation is a digital implementation of the assumed target and signal models.

Two variations of the specific scattering model are considered. The first target consists of both a low amplitude continuous scattering component, and two large amplitude point reflectors. In this model, the low level continuous scatterer is represented as a sequence of closely spaced point reflectors, whose reflection characteristics are random samples from uncorrelated Gaussian processes [2]. A second scattering model adds varying degrees of correlation to the continuous scatterer by filtering the uncorrelated sequence. The degree of correlation is inversely proportional to the bandwidth of the filter used, while the actual shape of the filter

response is relatively unimportant. SNR comparisons between the simulated correlated scattering values and the predicted levels, assuming uncorrelated scattering, for several filter bandwidths will be discussed.

Chapter 2 presents the analytic model for the range spread scattering function and receiver. The amplitude of the scattered signal is the convolution of the transmit pulse with the impulse response of the random target. For the thesis, it is assumed the medium may be modeled as a single deterministic propagation path with any randomness in the received signal due solely to the scattering process. The specific target model is characterized by a range spread scatterer [3]. The median reflection characteristics of the scatterer are specified by the range scattering function, $S(\tau)$, and is a function of delay only. The scattering function to be examined consists of two independent components, a low level continuous scatterer and a set of distinct, high amplitude point reflectors.

The response of the receiver to this signal is measured by the crossambiguity function, defined as the magnitude squared of the crosscorrelation between transmit and receiver processing signals. To simplify the form of the ambiguity function, both signals are assumed to be cosine pulses of frequency ω_c. The transmit pulse length is T_s, and the processing length T, where it is assumed $T > T_s$. Further, it is assumed target scattering process does not spread the signal in frequency, and for convenience, the scatterer

velocity is assumed to be zero. At zero Doppler and delay, the cross-ambiguity function reduces to simply the ratio of the transmit pulse length to the receiver integration time; i.e., T_s/T.

Clearly, if the scattering function were an ideal point reflector, the received signal would be simply a time delayed version of the transmit pulse, and the optimum receiver integration time corresponds to $T = T_s$ [4]. When the received signal is spread in time by the scattering process, this receiver integration time is suboptimum, or "mismatched." The performance, as measured by the signal-to-noise at the receiver output, will increase for some longer integration time, T, that best matches the received signal duration.

The simulation of the scattered signal and receiver are discussed in Chapter 3. Both models are derived from VanTrees [5]. The scattering function is obtained by combining the models for a range spread scatterer and a slowly fluctuating point target. The continuous scattering component is modeled as many closely, and equally, spaced point reflectors. The amplitudes of these reflectors are uncorrelated, complex Gaussian numbers of equal variance. The point reflectors are modeled by two uncorrelated, complex Gaussian numbers, with large variances compared to the continuous scatterers. For convenience, the point reflectors are placed along the scatterer so that the signal reflected from these points are separated by at least a transmit pulse length, i.e., the reflections from the point scatterers are resolved by the transmit pulse.

The receiver model used is shown in Figure 1. The reception, of either the reflected signal, or noise, is multiplied by the complex conjugate of the receiver processing signal, g(t), integrated and squared. It is assumed the signal and noise are uncorrelated, allowing the signal-to-noise ratio to be formed by passing the signal and noise through the receiver separately. By averaging many simulation outputs for signal or noise, a comparison statistic for the ambiguity function analysis may be generated.

A comparison of the simulated SNR, and that predicted by the ambiguity function analysis is presented in Chapter 4. The three combinations of the scattering model are 1) continuous scatterer, 2) composite scatterer, with both the continuous scatterer and point reflectors, and 3) point reflectors only. All comparisons are presented as a function of the ratio of the processing time, T, to transmit pulse length, T_s. The agreement between simulation and prediction is quite good, with an average difference of roughly 0.5 dB, independent of the specific type of scatterer, or the value of T/T_s.

Chapter 5 examines the effects of adding correlation to the continuous scattering component. Correlation is added by filtering the uncorrelated continuous scattering sequence, with the filter bandwidth inversely proportional to the degree of correlation in the filtered sequence. Comparing the predicted SNR with simulated values,

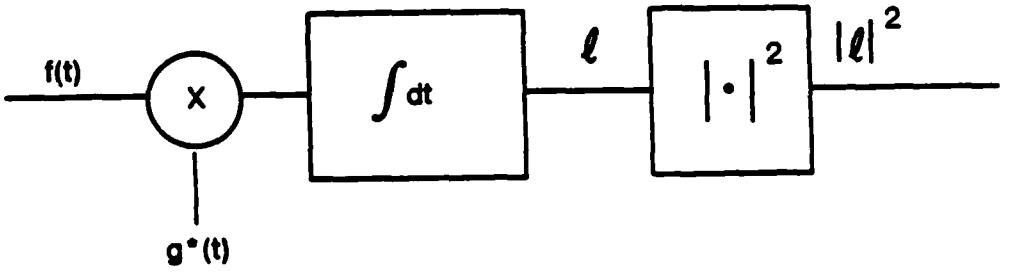

FIGURE 1. Block diagram of complex crosscorrelation receiver.

the quality of comparison decreases with decreasing filter bandwidth, or increasing correlation in the continuous scattering component. The correlated scatterer increases the received signal energy since the scattered signal now contains a coherent component as well as the random scatter. For very narrow bandwidths, the coherent return is large, and the simulated SNR is greater than the prediction for all values of T/T_s.

The effects of correlation on the continuous scatterer in the composite target is also compared with predicted SNR, assuming uncorrelated scattering. For a small degree of correlation, the comparison between simulated and prediction is affected only for data prior to the first point scatterer return. As with the continuous scatterer only comparisons, the simulated values are higher than the prediction, but this effect is overshadowed by the point scatterer returns for relatively wide filter bandwidths. For the very narrow bandwidth, the correlated, or coherent, scatterer energy obscures even the point scatterer returns, with differences between simulation and prediction as great as 17 dB. As with the correlated continuous scatterer only, the added energy due to the correlated scatterers is independent of T/T_s.

A summary of the major sections of this thesis is presented in Chapter 6. A number of areas for additional research are also discussed.

CHAPTER 2

MODEL ANALYSIS USING SCATTERING AND AMBIGUITY FUNCTIONS

2.1 Introduction

This chapter develops the analytic models for a range spread scatterer and complex correlation receiver. By specifying the form of the scattering function, transmitted pulse and receiver processing signal, the expected performance of the receiver may be evaluated analytically in terms of the scattering function and receiver ambiguity function. Performance is measured in terms of the receiver output SNR, for a given transmit pulse length T_s, and receiver processing time, T.

2.2 Complex Envelopes and Narrowband Signals

The waveforms considered in this thesis are restricted to the real signals that satisfy the relation

$$s(t) = \mathrm{Re}\left\{\tilde{s}(t)e^{j\omega_c t}\right\} \tag{2.1}$$

where $\tilde{s}(t)$ is the complex envelope of the signal, s(t), and ω_c is the signal carrier frequency in radians/second. These signals have Fourier transforms centered about $\pm\,\omega_c$, and are referred to as narrowband [6].

A property of narrowband signals is that the complex envelope is a slowly varying function compared to the carrier frequency. It is convenient to use the complex envelope for linear filter operations, and then take the real part of the output to recover the real output signal [7]. The narrowband signals of concern in this thesis are the transmit signal, f(t), and the receiver processing signal, g(t). Further it is assumed that both signals are pulsed cosines of the form;

$$f(t) = g(t) = \mathrm{Re}\left\{Ae^{j\omega_c t}\right\}, \quad 0 < t < T_1 \qquad (2.2)$$
$$= 0 \qquad , \text{ elsewhere}$$

where A represents the constant signal amplitude. These signals are energy normalized by assuming

$$\int_0^{T_1} \left|f(t)\right|^2 dt = 1 \qquad (2.3)$$

Combining Equations 2.2 and 2.3 yields

$$f(t) = \frac{1}{\sqrt{T_1}} \mathrm{Re}\left\{e^{j\omega_c t}\right\}, \quad 0 < t < T_1 \qquad (2.4)$$

2.3 The Range Scattering Function

2.3.1 Definition. The received signal is assumed to be the convolution of the transmit waveform f(t), with one realization of the time varying impulse response. While in general, the scattering

process may disperse the transmit signal in both time and frequency, the scatterer is considered to be stationary in this thesis. The reflected signal is delayed and temporally dispersed without any Doppler, or frequency spread. This type of scattering process is referred to as range-spread [8].

A physical model of the range-spread scatterer might be a line segment whose surface is random and rough compared to the wavelength of the transmit signal. The signal reflected from any increment, ΔL, along the scatterer is

$$\tilde{s}(t) = \sqrt{E_T}\, \tilde{f}(t-\tau)\, \tilde{b}(\Delta\tau) \tag{2.5}$$

where E_T is the energy in the transmit pulse, and $\tilde{f}(t-\tau)$ is the complex envelope of the transmit signal, delayed by τ. $b(\Delta\tau)$ is a sample function from a random reflection process and $\Delta\tau = 2\Delta L/c$, and c is the speed of sound.

The projected extent of the scattering function is assumed to be much greater than the transmit pulse length and independent of aspect angle. The reflected signal is then of greater duration than the transmit pulse, or spread in range by the target. The reflected signal is the superposition from many locations along the target. The signal at some time t is written,

$$\tilde{s}(t) = \sqrt{E_T} \sum_{i=1}^{N} \tilde{f}(t-\tau_i)\, \tilde{b}_i\,(\tau_i)\, \Delta\tau_i \tag{2.6}$$

where $\Delta\tau_i$ represents the time delay from the ΔL_i increment along the target. It is assumed that the number of scatterers along any increment is large so that $\tilde{b}(\tau)$ is a sample function from a complex Gaussian process [9].

The statistics of the received signal are completely specified by the mean value and the covariance function of the random range spread scatterer $\tilde{b}(\tau)$. The covariance function of the reflection process, $\tilde{K}(\tau,\tau_1)$ is defined as [10]

$$\tilde{K}(\tau,\tau_1) = E\left\{\tilde{b}(\tau)\tilde{b}^*(\tau_1)\right\} \tag{2.7}$$

The model is simplified further by assuming the reflection process is zero mean [11], and spatially uncorrelated. Equation 2.7 may then be written as,

$$\tilde{K}(\tau,\tau_1) = \delta(\tau-\tau_1) \cdot E\left\{\left|\tilde{b}(\tau)\right|^2\right\} \tag{2.8}$$

The range scattering function may now be defined as [12],

$$S_R(\tau) = E\left\{\left|\tilde{b}(\tau)\right|^2\right\} \tag{2.9}$$

The correlation function of the reflected signal in the absence of noise is,

$$\tilde{k}_s(\tau,\tau_1) = E\left\{\tilde{s}(\tau)\tilde{s}^*(\tau_1)\right\} \tag{2.10}$$

$$= E\left\{E_T \int_0^{T_T} \tilde{f}(t-\tau)\tilde{b}(\tau)d\tau \int_0^{T_T} \tilde{f}^*(t_1-\tau_1)\tilde{b}^*(\tau_1)d\tau_1\right\} \quad (2.11)$$

$$= E\left\{E_T \int_0^{T_T} \tilde{f}(t-\tau)\tilde{f}^*(t_1-\tau)\ S_R(\tau)d\tau\right\}, \quad (2.12)$$

for a scattered signal of duration T_T where $T_T \geq T_s$. The total energy in the signal reflected from a zero Doppler scatterer is [13]

$$E_R = \int_0^{T_T} \bar{K}_s(\tau,\tau_1)d\tau = E\left\{E_T \int_0^{T_T} S_R(\tau)d\tau\right\} \quad (2.13)$$

From Equation 2.13, note that the scattering function at any time delay, τ, represents the average energy reflected from a portion of the target at range, $r = c\ \tau/2$.

2.3.2 Composite Range Scattering Function. The particular scattering function of interest consists of two independent, random components. The first is a continuous scatter, characterized by a scattering density, ρ_E. The scattering function for the continuous component is a constant, or

$$S_{CS}(\tau) = \rho_E \quad (2.14)$$

where ρ_E is in units 1/seconds. The second scattering process is a set of large amplitude point scatterers. The point scattering function is

$$S_{HI}(\tau) = \sum_{i=1}^{N} E_i \, \delta(\tau-\tau_i) \tag{2.15}$$

where E_i represents the energy scattered from the i^{th} point scatterer. The total target scattering function is then,

$$S_R(\tau) = \rho_E + \sum_{i=1}^{N} E_i \delta(\tau-\tau_i) \tag{2.16}$$

Figure 2 is an example plot of the composite target scattering function for comparatively large point scatterer amplitudes and a low continuous scatter amplitude. Convolution of the scattering function and a 10 millisecond transmit pulse yields the reflected signal shown at the bottom of the figure.

2.4 Receiver Ambiguity Function

2.4.1 Receiver Model. The receiver used to process the signal reflected from the composite scatterer is shown in Figure 1, and is defined by VanTrees as the complex correlation receiver [14]. For detection, the reflected signal is multiplied by the conjugate of the receiver processing waveform, g(t), integrated for a time T, magnitude squared, and the output compared with a threshold.

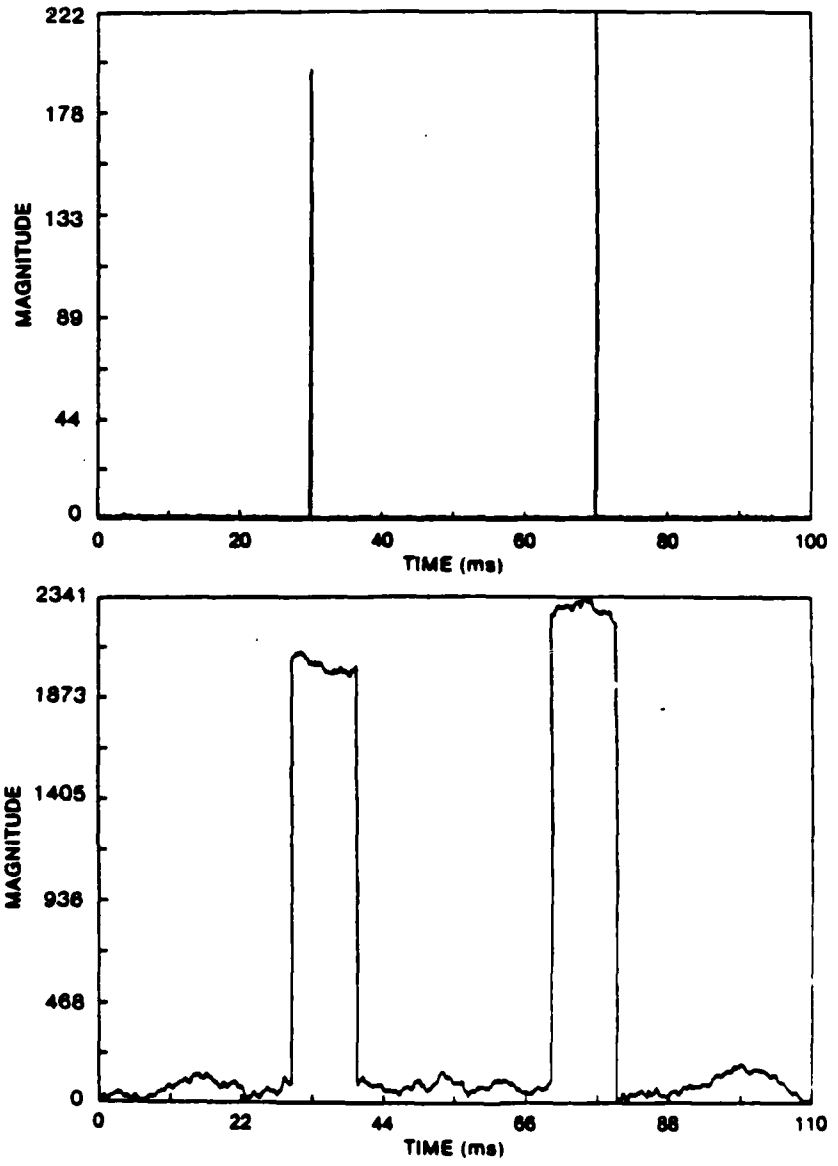

FIGURE 2. Magnitude of the composite scattering function (top), and reflected signal (bottom). Note the difference between the time axes.

The performance of the receiver is calculated as a function of the integration time to pulse length ratio, $T/T_s \geq 1$, and is measured by the ratio of the mean signal energy to mean noise energy at the receiver output. The output SNR is then defined as

$$SNR = \frac{E\{s(t)s^*(t)\}}{E\{n(t)n^*(t)\}} . \tag{2.17}$$

Noise is assumed to be a white, band limited, Gaussian noise of power spectral density N_0. The output noise energy is

$$E_N = N_0 \int_0^T \left|g(t)\right|^2 dt = N_0 , \tag{2.18}$$

which is numerically equal to the the spectral density by Equation 2.3.

2.4.2 Receiver Ambiguity Function. A measure of the receiver response to a returned signal is the crossambiguity function defined as

$$\left|\chi(\tau,\omega)\right|^2 = \left|\int_{-\infty}^{\infty} \tilde{f}(t-\tfrac{\tau}{2})\tilde{g}^*(t+\tfrac{\tau}{2})e^{j\omega t}\, dt\right|^2 . \tag{2.19}$$

Note that the term

$$\chi(\tau,\omega) = \int_{-\infty}^{\infty} \tilde{f}(t-\tfrac{\tau}{2})\tilde{g}^*(t+\tfrac{\tau}{2})\, e^{j\omega t}\, dt \tag{2.20}$$

is the crosscorrelation of the transmit and processing signals, and indicates the "match" between the reflected signal and transmit signal [15].

For the assumed transmit signal and receiver model, Equation 2.2, the crossambiguity function is derived in Appendix A as

$$\left|X(\tau',\omega')\right|^2 = \frac{T_s}{T}\left[\frac{\sin\left(\frac{\omega' T_s}{2}\right)}{\frac{\omega' T_s}{2}}\right]^2 \qquad \text{(A-9)}$$

where τ' and ω' are defined in Appendix A for zero Doppler, Equation A-9 reduces to simply T/T_s, a constant.

The signal-to-noise ratio may now be written in terms of the scattering and ambiguity functions as,

$$SNR = \frac{\int_{-\infty}^{\infty}\left|X(\tau',\omega')\right|^2 S_R(\tau')\, d\tau'}{N_0} . \qquad (2.21)$$

Substituting Equation 2.16 into 2.21 yields

$$SNR = \frac{\int_0^{T_T}\frac{T_s}{T}\left(\rho_E + \sum_{i=1}^{N} E_i\delta(\tau-\tau_i)\right)d\tau}{N_0} \qquad (2.22)$$

$$= \frac{1}{N_0}\left[\frac{\rho_E T_s T_T}{T} + \frac{T_s}{T}\sum_{i=1}^{N} E_i\right] . \qquad (2.23)$$

Equation 2.23 predicts the mean signal to mean noise ratio as a function of transmit and processing pulse lengths. It may be evaluated numerically by knowing the scattering strengths ρ_E and E_i for a particular scatterer.

CHAPTER 3

SIMULATION OF TARGET AND RECEIVER MODELS

3.1 Simulation of the Composite Scattering Function

3.1.1 Simulation of a Continuous Scatterer. The model for a range spread scatterer from VanTrees [16] is used to simulate the continuous scatterer. The continuous scatterer is modeled as a line of equi-spaced point scatterers, each with a random amplitude drawn from independent zero-mean, complex, Gaussian processes with variance, σ_{cs}^2. A complex Gaussian process is defined as

$$\tilde{r}(n) = \tilde{r}_R(n) + j\,\tilde{r}_I(n) \tag{3.1}$$

where r_R and r_I are sample functions from real Gaussian variables. It is assumed that $\tilde{r}_R$ and $\tilde{r}_I$ are uncorrelated, so that

$$E\left\{\tilde{r}_i(n)\tilde{r}_j^*\right\} = 0, \quad \text{for } i \neq j\ , \tag{3.2}$$

The continuous scatterer is approximated by 1000 point scatterers, each of variance σ_{cs}^2, and separated by $1/f_s$ = .01 ms, where f_s is the digital sampling frequency in Hertz. The variance of each point in the continuous scatterer is related to the continuous scattering density, ρ_E, by

$$\rho_E = \sigma_{cs}^2\, f_s^2\ . \tag{3.3}$$

3.1.2 Simulation of Point Scatterers. The model for the point scattering component is the slowly fluctuating point target, defined by VanTrees [17]. The simulation model is specified by fixing the location of the point scatterers along the length of the continuous scatterer. For the purposes of this thesis, the point scatterers are fixed at sample locations 300 and 700, on the 1000 sample continuous scatterer. It is assumed the amplitudes of the point scatterers are sample functions of zero mean, uncorrelated Gaussian process, with equal variance, σ_{HI}^2, where $\sigma_{HI}^2 > \sigma_{cs}^2$.

To calculate the energy reflected from the point scatterers, the length of the transmit pulse is restricted to

$$T_s < \frac{700-300}{f_s} = 40 \text{ ms} \tag{3.4}$$

where 300 and 700 are the sample numbers corresponding to the location of the two point scatterers. Equation 3.4 implies the transmit pulse length is short enough to resolve the point reflections, though not the scatterers in the continuous scatterer, and the average energy in N point scatterer reflections is then N times the energy of a single point reflection.

3.2 Generation of Simulated and Predicted SNR

3.2.1 Simulation of Reflected Signal. To generate the simulated signal reflection from the composite scatterer, many realizations of the random scattering process, whose mean reflection characteristics are described by the scattering function, are required. Each sample of this random process is obtained from a Gaussian random number generator, described in Appendix B, assuming zero mean, and a standard deviation of σ_{CS}, σ_{HI} or σ_{N}, depending on the scattering component required. To simulate the composite scatterer in noise, the outputs of three independent random number sequences, one for each random component, are added to form a single realization of the random composite scatterer. The envelope of the transmit signal is the convolved with this random sequence to produce a representation of the signal reflected from the random, range-spread, composite scatterer. This signal is passed through the correlation receiver, and the average of many receiver outputs compared to the predicted output. The convolution is accomplished by Fourier transforming the transmit and scattering sequences, multiplying them together, and performing an inverse Fourier Transform. The size of the FFT is determined by

$$NFFT = 2\ [LOG10(NT_S+NTAR)/ALOG(2)] + 1 \qquad (3.5)$$

where $NT_S = T_s \cdot f_s$ and NTAR = 1000. The result is a sequence 1099 samples long, with samples 300 to 400 and 700 to 800 representing the point reflector returns. Table 1 lists the simulation parameters that are constant for all runs, including the durations of the transmit signal and continuous scatterer.

Noise is assumed to be zero mean, white and Gaussian. It is simulated identically to the continuous scattering sequence discussed in Section 3.1.1, with the noise spectral density equal to the variance of each point in the random noise sequence.

The simulation of sequences of random numbers, both for the scattering process and noise is discussed in Appeddix B.

3.2.2 Generation of Simulated and Predicted SNR. To calculate the simulated SNR, each realization of the reflected signal is passed through the digital equivalent of the receiver shown in Figure 1, for a given number of samples NT, where $NT = T \cdot f_s$. J realizations of the signal, and J realizations of noise are passed through the receiver separately, with the mean signal-to-noise ratio computed by

$$SNR = \frac{\bar{S}}{\bar{N}} \cdot \frac{\sum_{K=1}^{J} |S_K|^2}{\sum_{K=1}^{J} |N_K|^2} \qquad (3.6)$$

Table 1 - Constant Simulation Scattering and Receiver Model Parameters.

- Continuous scatterer length = 100 ms
- Transmit pulse length = 10 ms
- Sampling rate = 10000 Hz
- Number of highlight scatterers = 2
- Location of highlights = 30 and 70 ms
- Minimum Receiver Integration Time = 10 ms

where $|S_K|^2$ is the $K^{\underline{th}}$ receiver output for signal only and $|N_K|^2$ is the $K^{\underline{th}}$ output for noise only.

The predicted SNR is evaluated by relating the terms in the SNR prediction equation, Equation 2.23, to the variance of each of the scattering and noise variances, or

$$SNR = \frac{1}{\sigma_N^2}\left[\sigma_{cs}^2 f_s^2 T_s + \frac{T_s}{T}\frac{N}{N_{HI}}\sigma_{HI}^2\right] \qquad (3.7)$$

where N is the number of samples of the point scatterer returned in the interval [0,T] and $0 < N/NTS < 2$. σ_N^2 is the variance of the zero mean, Gaussian, noise process.

As noted earlier, the range of T/T_s values discussed in the thesis are between 1 and 11. For simplicity, it is assumed that any bulk delay in the reflected signal is known, so that the receiver begins processing the reflected signal at the onset of the continuous scatterer return, $T/T_s = 0$. The first comparison between simulation and Equation 3.7 is made at $T/T_s = 1$, after an entire transmit pulse duration has been processed through the correlation receiver. This method of fixing the processing start time is followed throughout the

thesis, whether the continuous scatterer return is present or not. In particular, the examples shown in Section 4.3, point scatterers in noise, begin at $T/T_s = 4$, one transmit pulse length after the first point reflector return at $T/T_s = 3$, with the receiver output from $T/T_s = 1$ to $T/T_s = 2.5$ representing noise only.

In addition, the energy in the signal reflected from the continuous scatterer is not constant with increasing integration time, as implied by in Equation 3.3, and the relationship of the continuous scattering variance to the continuous scattering density must be modified to account for the time spread of the reflected signal. The received signal is the convolution of the transmit signal, say N points long, and the target, M points long, where M > N. The resulting sequence is M+N-1 long. In Figure 2, note that the received signal duration is roughly 0.11 sec, for a scattering function 0.1 sec long and a 0.01 sec transmit pulse. The variance of the signal, assuming uncorrelated point scatterers is

$$\sum_{i=1}^{M} N^2 \sigma_{cs}^2 = M \cdot N^2 \sigma_{cs}^2 \qquad (3.8)$$

However, the leading and trailing edges are ramp functions of the form

$$\sigma_{EDGE}^2 = \frac{N}{2} (N+1) \sigma_{cs}^2 \qquad (3.9)$$

The variance of the first N samples of the reflected signal, for a transmit pulse length of N samples, is not $N^3 \cdot \sigma_{cs}^2$ but,

$$\sigma_{EDGE}^2 = (N^3 - \frac{N}{2}(N+1))\ \sigma_{cs}^2 \qquad (3.10)$$

Equations 3.9 and 3.10 are then used as corrections for calculations of the continuous scattering energy in Equation 3.7.

CHAPTER 4

COMPARISON OF PREDICTED AND SIMULATED SNR

4.1 Introduction

4.1.1 Introduction. In this chapter, the comparison of the predicted and simulated SNR is presented. Fourteen combinations of scattering strength parameters are presented. These cases cover small and large point scatterer reflectivities, and both high and low signal-to-noise. The standard deviation of the scattering strength parameters are listed in Table 2, along with some statistics of the differences between predicted and simulated SNR. The constants for all the simulation trials are transmit pulse length, T_s, continuous scatterer duration, point scatterer position along the continuous scatterer and the number of independent realizations of the model averaged to compare with the SNR predicted from Equation 3.8.

Table 2 lists the scattering strength parameters and some statistics of the differences between predicted and average simulation SNR, for the fourteen scattering strength parameters examined. Columns 2-4 list the standard deviation of the scattering and noise components of Equation 3.7. Columns 5-7 list the maximum difference between simulation and prediction, the geometric mean difference between prediction and simulation, and the standard deviation of the difference, respectively, for each set of scattering strength parameters.

TABLE 2 - Scattering Strength Parameters and Statistics of Differences between Simulated and Predicted and Simulated Signal-to-Noise Ratios for 14 Combinations of Scattering Strength Parameters.

	STANDARD DEVIATION OF SCATTERING PARAMETERS			DIFFERENCES BETWEEN MODEL AND THEORY (Average of all values of T/T_S.)		
CASE NO.	σ_{CS}	σ_{HI}	σ_N	MAX DB	MEAN DB	ST. DEV. DB
1	1.	0.	1.	1.1	0.4	0.3
2	0.	1.	1.	1.0	0.4	0.3
3	100.	0.	1.	1.1	0.5	0.3
4	0.	100.	1.	1.2	0.5	0.3
5	1.	0.	100.	1.6	0.6	0.4
6	0.	1.	100.	1.7	0.4	0.4
7	1.	10.	1.	1.2	0.5	0.3
8	1.	100.	1.	1.3	0.5	0.3
9	1.	100.	100.	1.4	0.6	0.3
10	1.	1.	1.	1.5	0.5	0.4
11	1.	0.	1000.	0.9	0.3	0.3
12	1.	100.	1000.	2.2	0.4	0.5
13	1.	0.	9500.	1.4	0.6	0.4
14	1.	100.	9500.	1.1	0.4	0.4
	AVERAGE			1.3	0.5	0.3

The mean difference between theory and Equation 3.7 is defined as the geometric average of differences at each value of T/T_s examined, in decibels, for a set of scattering strength parameters, or,

$$\bar{E}(dB) = \frac{1}{N} \sum_{i=1}^{N} E_i \ (dB) \tag{4.1}$$

where E_i is the absolute value of the difference of the predicted SNR and the simulated SNR, in dB, for a particular value of T/T_s. Similarly, the standard deviation of differences is computed by

$$\sigma_{DATA} \ (dB) = \left[\frac{1}{N} \sum_{i=1}^{N} [E_i - \bar{E}]^2 \right]^{1/2} \tag{4.2}$$

4.1.2 Calculation of Comparison Data. For a particular set of scattering strength parameters σ_{cs}, σ_{HI}, σ_N, Equation 3.7 is used to generate the theoretical SNR prediction for receiver integration times from equal to the transmit pulse length, T/T_s = 1.0, to T/T_s = 11, which encompasses the entire scattered signal. The prediction equation is evaluated at increments of one-half the transmit pulse length between these two values.

The simulation SNR is also generated for each set of scattering strength parameters, and the 21 values of T/T_s between 1.0 and 11. 100 realizations of the random model, which are assumed to be independent since each starts with a unique seed value, are linearly

averaged. Ten times the logarithm of the average value is then compared with the predicted value.

It is important to note that the statistics of the differences between theory and model listed in Table 2 are calculated using only 19 of the receiver integration times between T/T_s = 1.0 and 11. Due to the point scatterer return at T/T_s = 3.0, the differences between model and prediction equation at T/T_s = 3.0 and 3.5 are not included. At these integration times, the received signal includes a statistically small number of samples from the large variance, highlight return, and therefore displays large fluctuations, even after averaging 100 simulation realizations. Not until a complete transmit pulse is processed by the receiver, is a comparison between the predicted result, and the scattering model output, considered valid.

4.1.3 Presentation of Comparison Data. In addition to the results listed in Table 2, two types of graphical comparisons are used. An example of the first plot type is shown in Figure 3, with SNR on the ordinate, and T/T_s on the abscicca. The theoretical SNR prediction is shown as circles, and the model average SNR depicted by squares. Note the data points at T/T_s = 3.0 and 3.5 are shown in this figure, though they are not included in the statistical comparisons listed in Table 2.

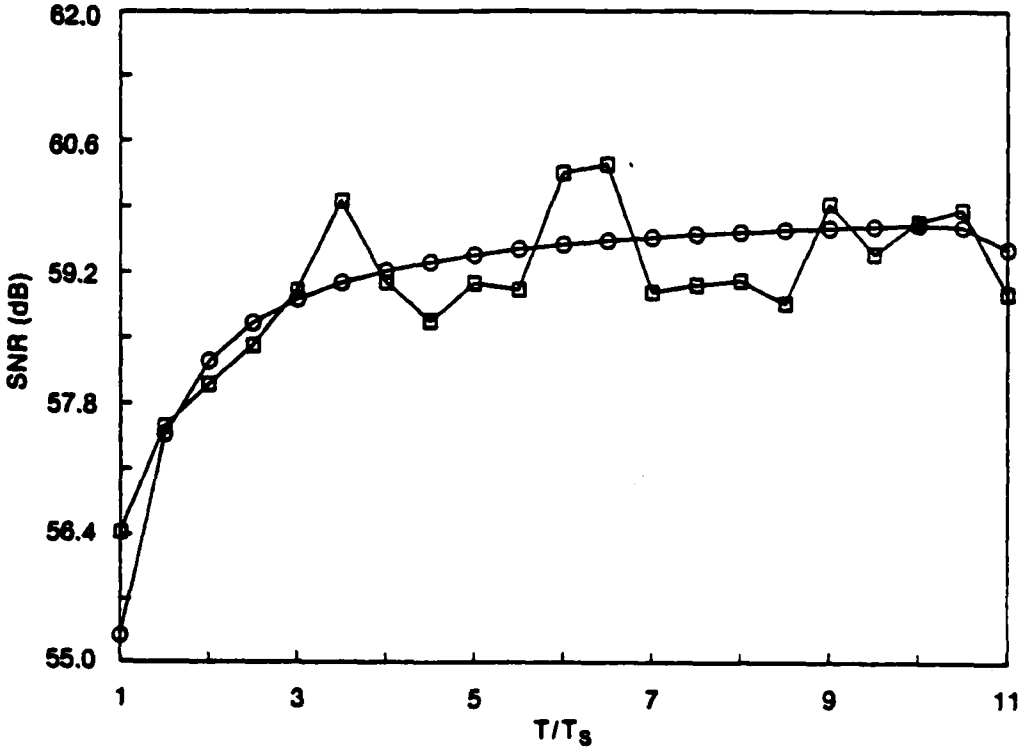

FIGURE 3. Comparison of predicted and simulated SNR for Case 1; $\sigma_{CS} = 1$, $\sigma_{HI} = 0$, $\sigma_N = 1$. Predicted values are shown as circles, simulated data shown as squares.

The second type of graph is shown in Figure 4. As in Figure 3, the predicted values are shown as circles, and the simulation data as squares. The abscicca axis is the ratio of transmit pulse length to receiver integration time, T/T_s. The ordinate is SNR, normalized by the predicted SNR. Thus the predicted values appear to lie on a horizontal line at 0 dB. The vertical bars around the normalized simulation data depict the 90 percent confidence interval to be discussed in Section 4.2.

4.2 The Continuous Scatterer in Noise

4.2.1 Continuous Scatterer in Noise. The simplest realization of the model is the continuous scatterer only in the presence of low background noise. Figure 3 is a SNR versus T/T_s plot, for Case 1, a high SNR combination of scattering strength parameters (see Table 2). The maximum predicted SNR occurs at a value of $T/T_s = 10.5$. The simulation SNR values generally follow the prediction curve, with a maximum difference between the two curves of 1.1 dB, and a mean difference of 0.4 dB.

The prediction curve has maximum slope for T/T_s values less than 4.0. The slope of the SNR versus T/T_s curve is important, since it indicates the region of receiver integration times that yield the greatest increase in SNR, for the least increase in integration time. This behavior is intuitively correct, since increasing the integration time from $T/T_s = 1.0$ to 2.0, doubles the amount of

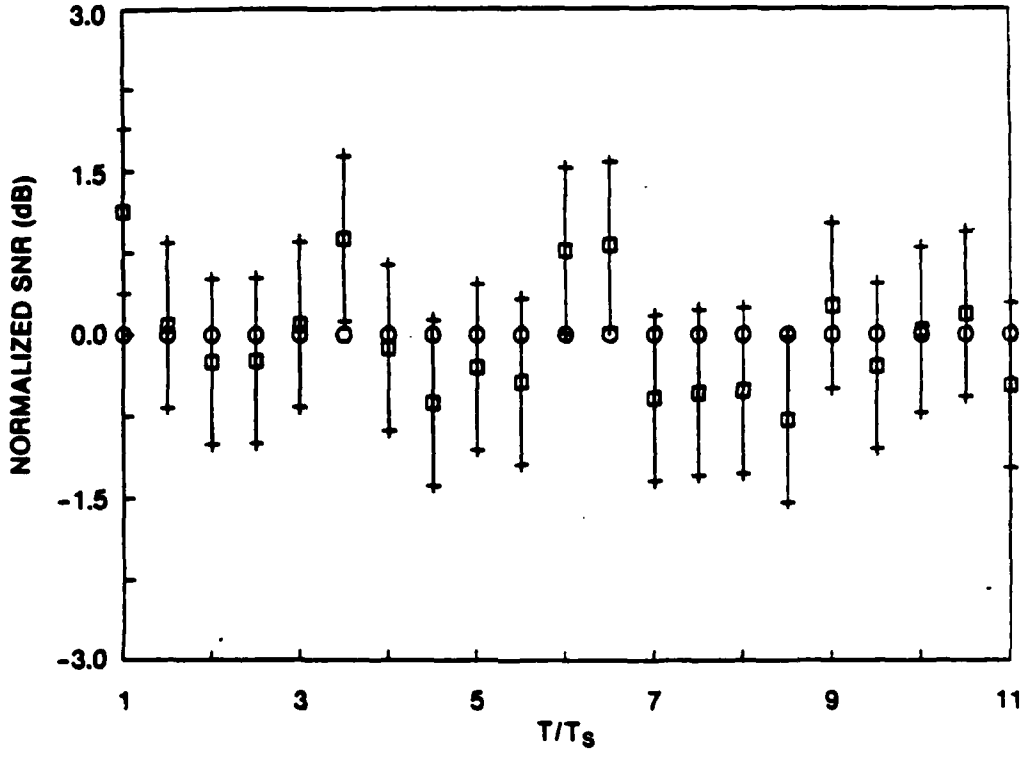

FIGURE 4. Comparison of normalized SNR for Case 1; $\sigma_{CS} = 1$, $\sigma_{HI} = 0$, $\sigma_{N} = 1$. Predicted values are shown as circles, simulated data shown as squares.

signal energy processed by the receiver. Conversely, increasing the listen "window" from T/T_s = 10.0 to 11.0 adds only ten percent more signal energy.

4.2.2 Distribution of Simulated SNR. The ambiguity - scattering function analysis presented in Chapter 2 allows calculation of the mean SNR for a given set of scattering parameters and pulse lengths, but contains no information concerning the distribution of SNR about the mean. Using VanTrees' models for noise and the continuous scatterer, it is possible to derive the distribution of simulated SNR.

The essence of the derivation is that both received signal and noise are modeled as independent, zero mean, Gaussian processes. The quantity of interest, SNR, is the ratio of received signal squared and noise squared. The SNR is then the ratio of two chi-squared variables, and the distribution of this ratio is the F distribution. The interested reader is referred to Appendix C for the complete derivation.

Knowing the distribution of SNR, the confidence limits of the simulated data may readily be computed. Figure 4 is a plot of normalized SNR versus T/T_s for the case shown in Figure 3. As noted previously, both the simulated and predicted SNR values are normalized by the predicted SNR, which transform the prediction curve in Figure 3 to the horizontal line in Figure 4. For 90 percent confidence, the simulated values must lie within $\pm$ 0.75 dB of the predicted value.

This range is depicted in Figure 4 by the vertical bars through each of the normalized simulation data. Note in Figure 4 that three of the twenty-two normalized simulation values are not within the confidence bounds, roughly the number expected for 90 percent confidence.

Also it is worth noting that the confidence intervals for the matched filter condition are not strictly correct. For $T/T_s = 1$, the received signal builds from one sample at $t = 0$ to the sum of N scatterers at $t = T_s$. The sequence is triangular, with each sample increasing in degrees of freedom with time. The total number of degrees of freedom in this sequence are not the same as the rest of the received signal, which results in a slightly wider confidence interval than the ± 0.75 dB for values of $T/T_s \neq 1$.

4.2.3 Comparison as a Function of SNR. The comparison between simulation and prediction appears to be unaffected by the absolute SNR. In addition to the case discussed above, three other combinations of continuous scattering strength and noise were examined, with the predicted SNR between -20 to +95 dB. Representative examples are shown in Figures 5 and 6.

Note Figures 5 and 6 indicate only small differences between model and theory for the case of equal continuous scattering strength and noise spectral density, i.e., 0 dB. The largest difference between prediction and simulation is 1.3 dB, and as can be seen in

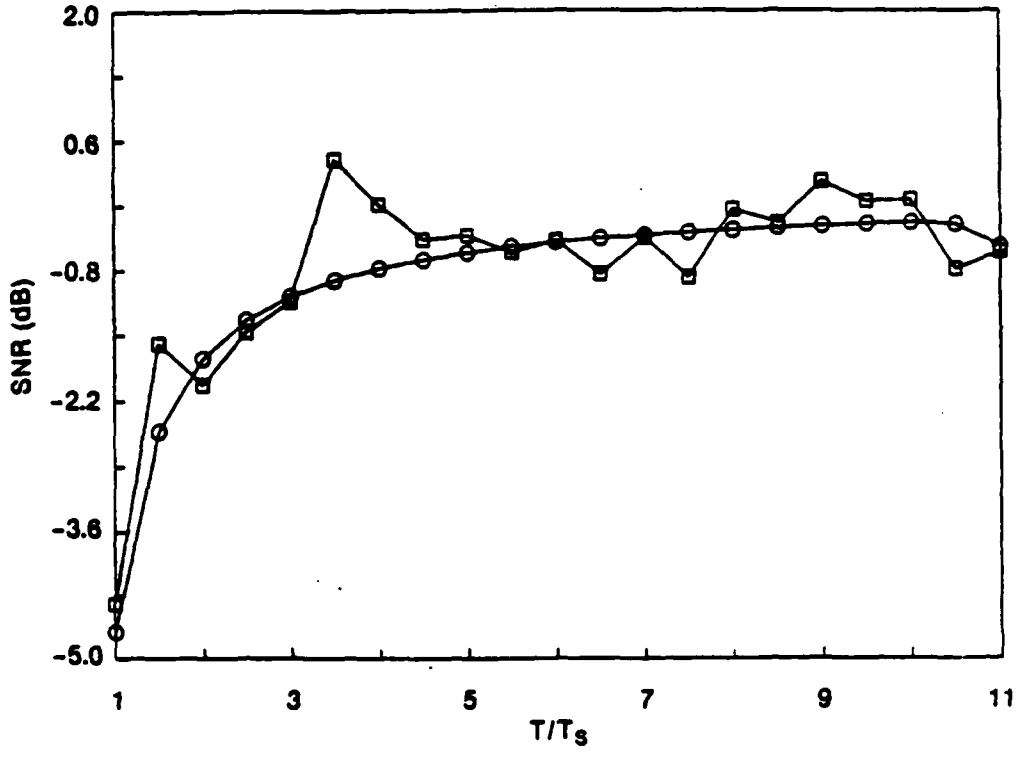

FIGURE 5. Comparison of predicted and simulated SNR for Case 11; $\sigma_{CS} = 1$, $\sigma_{HI} = 0$, $\sigma_N = 1000$. Predicted values are shown as circles, simulated data shown as squares.

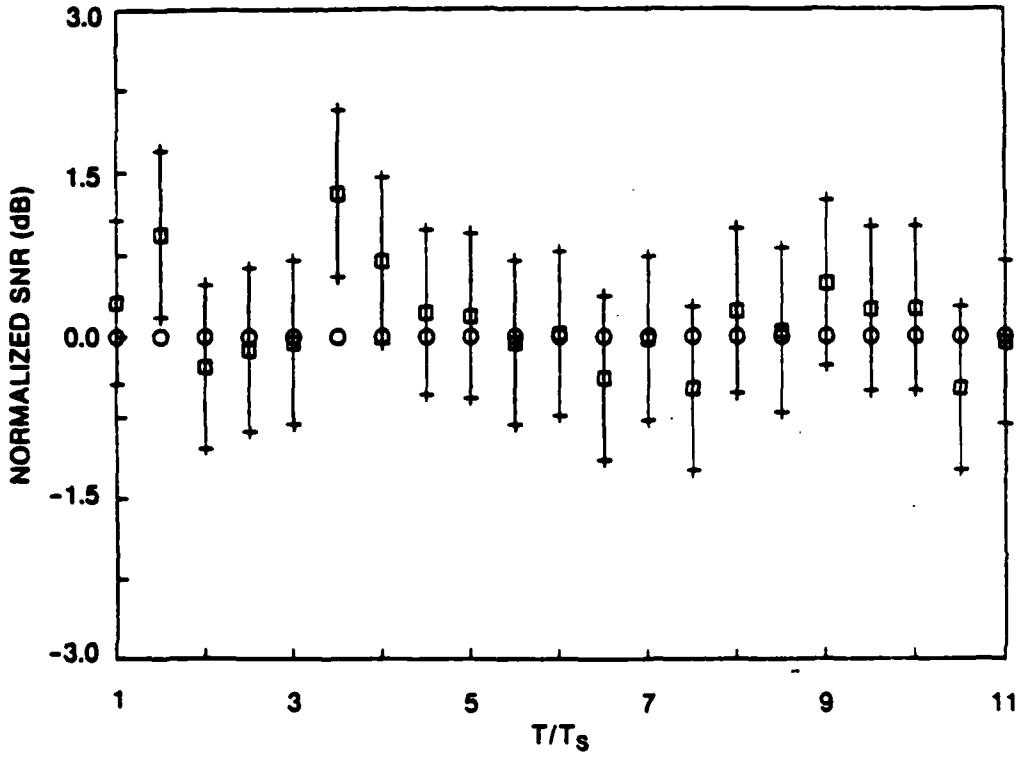

FIGURE 6. Comparison of normalized SNR for Case 11; $\sigma_{CS} = 1$, $\sigma_{HI} = 0$, $\sigma_N = 1000$. Predicted values are shown as circles, simulated data shown as squares.

Figure 6 only two of the data points, at T/T_s = 1.5 and 3.0, fall outside the 90 percent confidence interval. Similar results were observed for for both very low SNR, -20 dB, and very high SNR, +95 dB.

4.3 Point Reflectors in Noise

The other components of the composite scatterer are the two point reflectors. Figure 7 is a plot of SNR versus T/T_s, for two moderately large point scatterer returns in noise. Since the point scatterer return does not begin until T/T_s = 3.0, comparisons between the model and theory are not considered valid until T/T_s = 4.0. Note that abscicca values in Figures 7-10 begin at 4.0 for this reason.

Figure 7 is a SNR versus T/T_s plot for the two highlight reflectors in noise with a mean SNR of roughly 35 dB. As before, the predicted values are shown as circles, and the simulation values as squares or boxes. The largest difference between the two curves is 1.0 dB, with the average difference 0.4 dB, indicating that the model accurately follows the predicted values. Note that both curves are a maximum at T/T_s = 4.0 and 8.0, corresponding to receiver integration times that receive the entire point scatterer reflection and minimum noise energy. Between the first and second point reflections, and after the second point reflection, the SNR drops off due to the addition of noise, and the lack of any additional signal energy.

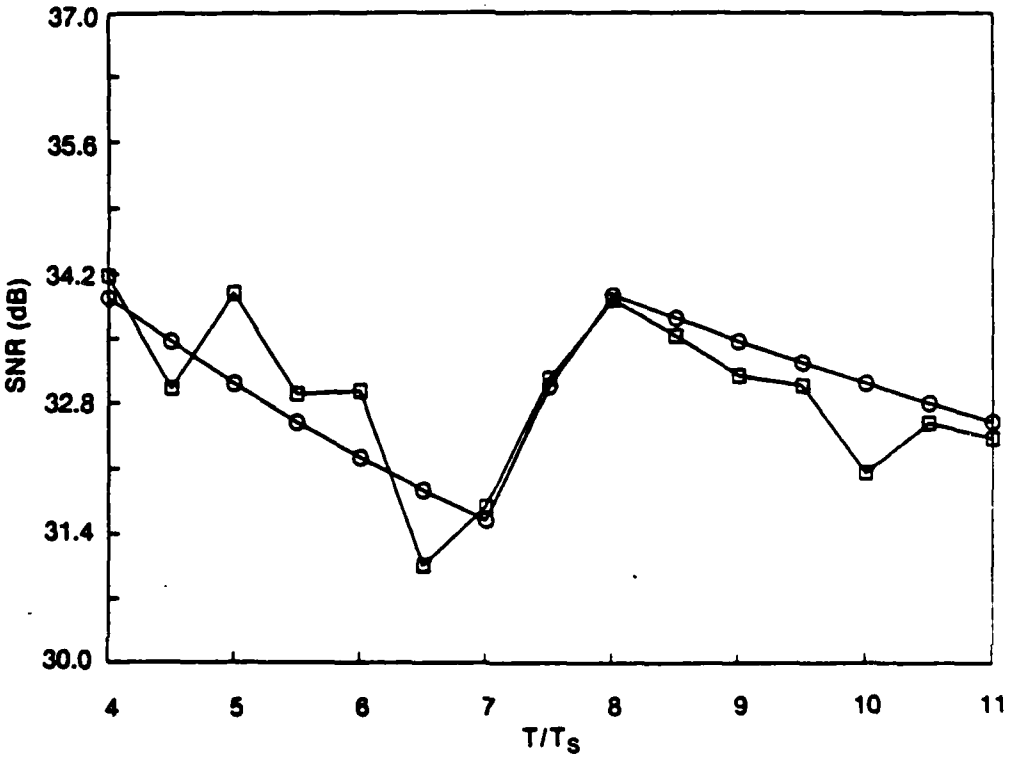

FIGURE 7. Comparison of predicted and simulated SNR for Case 2; $\sigma_{CS} = 0$, $\sigma_{HI} = 1$, $\sigma_N = 1$. Predicted values are shown as circles, simulated data shown as squares.

The good agreement between theory and model is also observed in the normalized SNR versus T/T_s plot, Figure 8. Three of 16 simulation values fall outside the confidence interval. No systematic or periodic differences between the two curves is apparent.

A low SNR case is shown in Figures 9 and 10. Note the rapid decrease in SNR between the point reflector returns when no continuous scattering component is present. Again, the simulated values of SNR closely follow the predicted values, and the normalized data, Figure 10, shows only a single point out of 16 outside the 90 percent confidence interval.

4.4 The Composite Scatterer in Noise

4.4.1 Composite Scatter in Noise. A complete realization of the model includes reflections from two point reflectors, of variance σ^2_{HI}, to the continuous scatterer return. The locations of the point scatterers are fixed to T/T_s values of 3.0 and 7.0. Two examples of the envelope of the signal reflected from the composite scatterer are shown in Figures 2 and 11. The point scattering strength in Figure 2 is 10 times the point scatterer strength in Figure 11, but in both cases, the variance of the point scatterers is large compared to the continuous scatterer and noise.

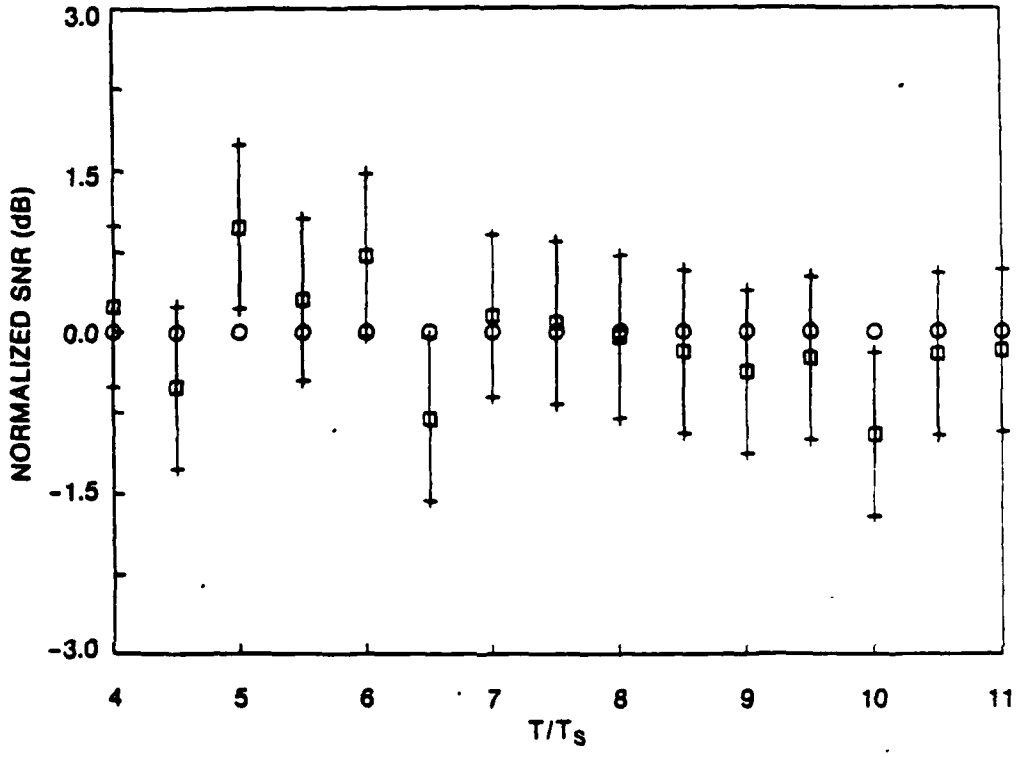

FIGURE 8. Comparison of normalized SNR for Case 2; $\sigma_{CS} = 0$, $\sigma_{HI} = 1$, $\sigma_N = 1$. Predicted values are shown as circles, simulated data shown as squares.

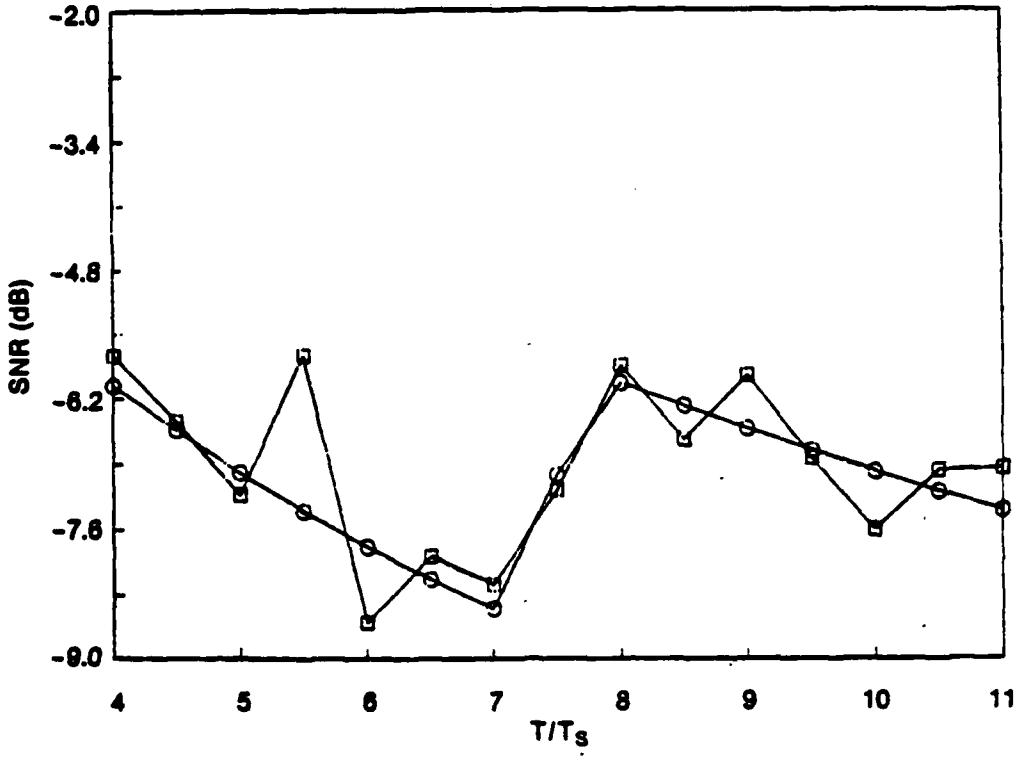

FIGURE 9. Comparison of predicted and simulated SNR for Case 6; $\sigma_{CS} = 0$, $\sigma_{HI} = 1$, $\sigma_N = 100$. Predicted values are shown as circles, simulated data shown as squares.

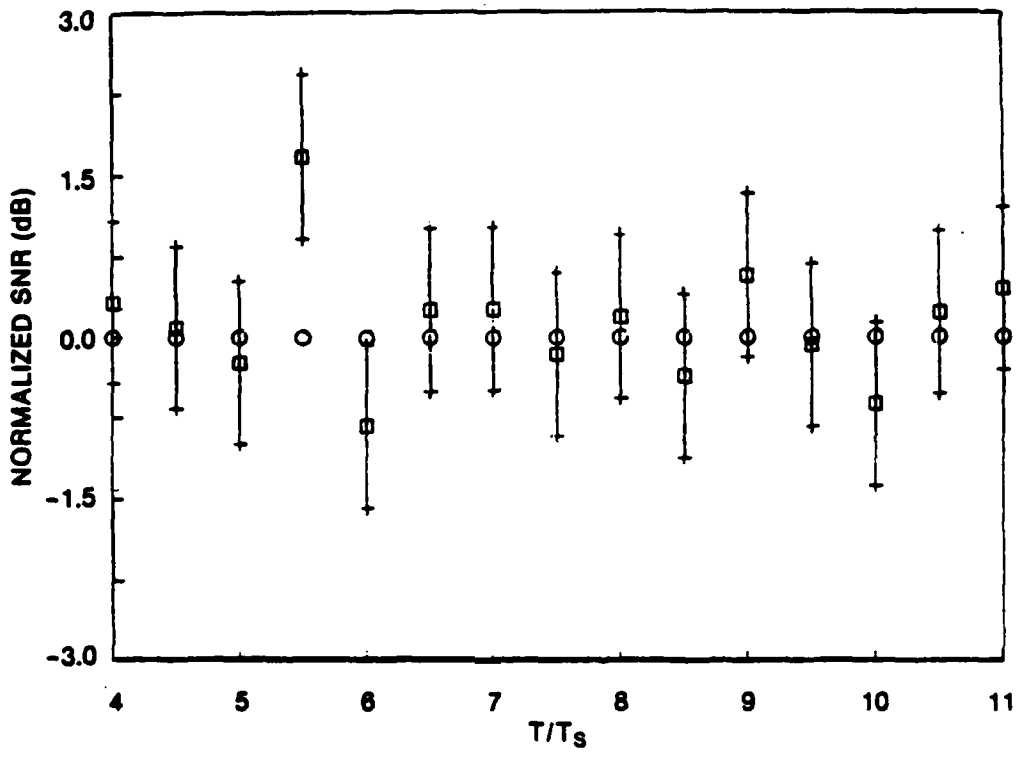

FIGURE 10. Comparison of normalized SNR for Case 6; $\sigma_{CS} = 0$, $\sigma_{HI} = 1$, $\sigma_N = 100$. Predicted values are shown as circles, simulated data shown as squares.

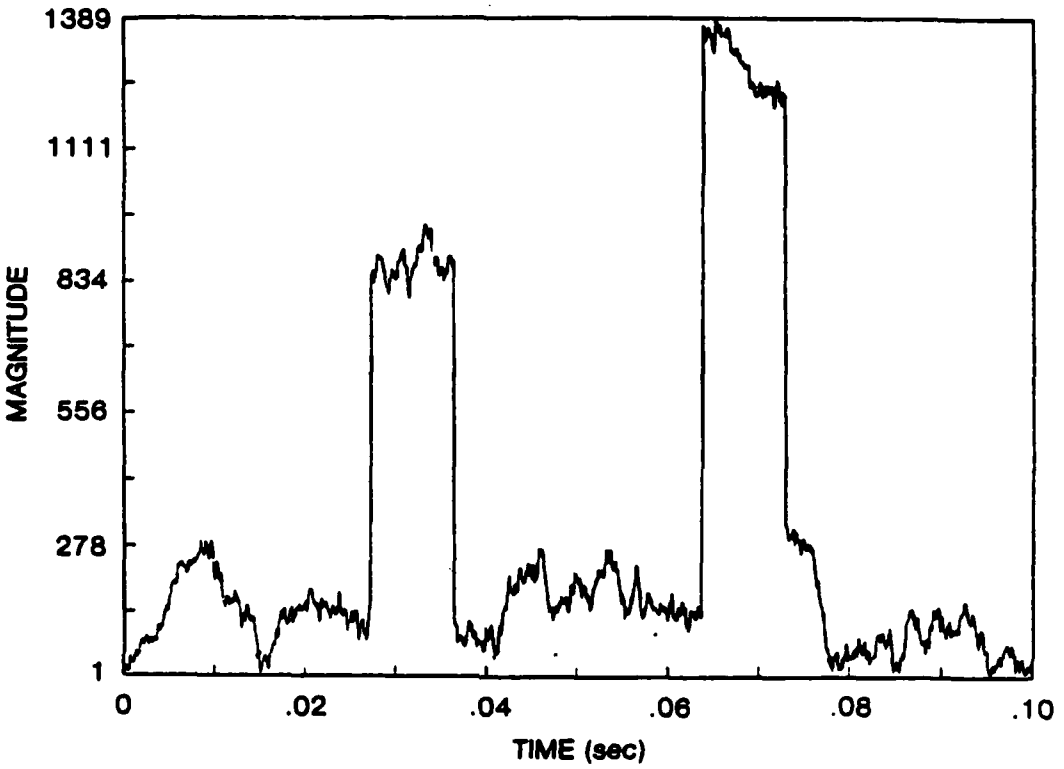

FIGURE 11. One realization of the signal reflected from the composite scatterer for large point scatterer reflectivity.

The SNR versus T/T_s plot for a high SNR, large point scatterer reflectivity case is shown in Figure 12. For values of T/T_s less than 3.0, the signal energy is due soley to the continuous scatterer. With the onset of the first point scatterer reflection, the SNR rapidly increases, with the prediction curve reaching a local maximum at $T/T_s = 4.0$. Between the point scatterer returns, the SNR falls off 3 dB, and reaches a second maximum with the arrival of the second point reflection. Differences between simulation and prediction for this example are roughly equal to the differences seen in the previous sections. Again neglecting data at $T/T_s = 3.0$ and 3.5, the average difference between the two curves is 0.5 dB, with a maximum difference of 1.3 dB, at a value of $T/T_s = 10.0$.

The normalized SNR plot for this example is shown in Figure 13. The majority of the normalized simulation values fall within the 90 percent confidence interval. Only the data at $T/T_s = 6.0$ and 10.0 are outsides these limits. It is important to note that the composite scatterer data, as well as the component scatterers individually, does not display any apparent pattern in the differences between simulation and prediction.

Figure 14 is a SNR versus T/T_s plot of composite scatterer data for point scatterer reflectivities 1/10 the strength of the example shown in Figure 12. The predicted SNR values for T/T_s less than 3.0 are the same in both Figures 12 and 14, though plotted on different scales. The onset of the first point scatterer reflection in Figure

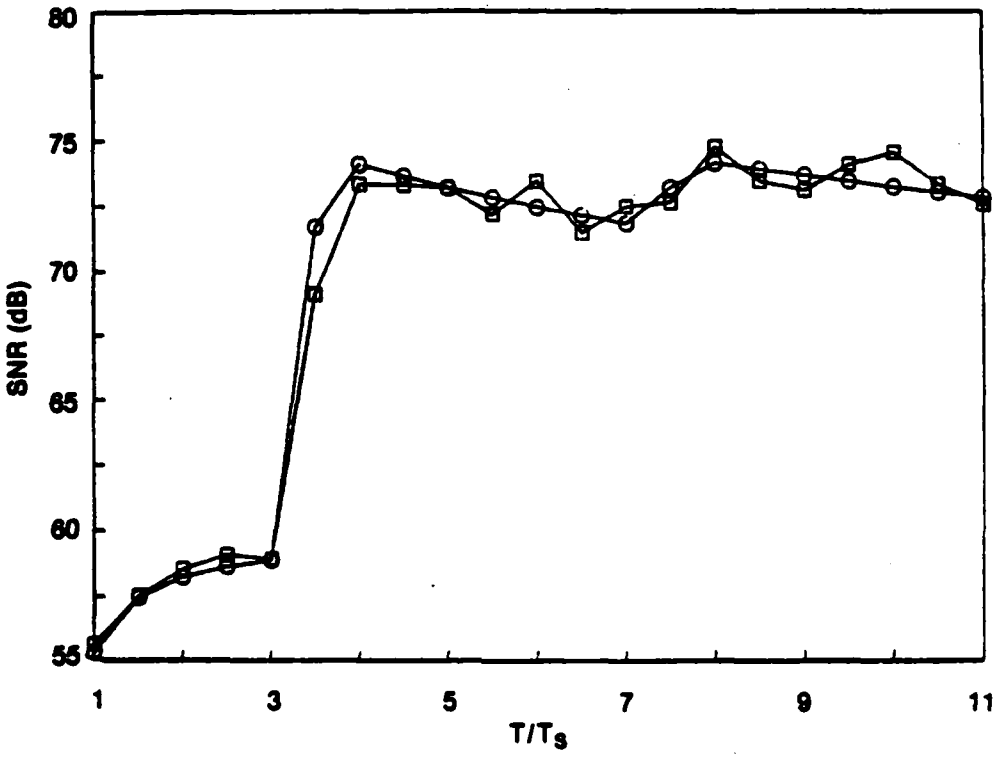

FIGURE 12. Comparison of predicted and simulated SNR for Case 8; $\sigma_{CS} = 1$, $\sigma_{HI} = 100$, $\sigma_N = 1$. Predicted values are shown as circles, simulated data shown as squares.

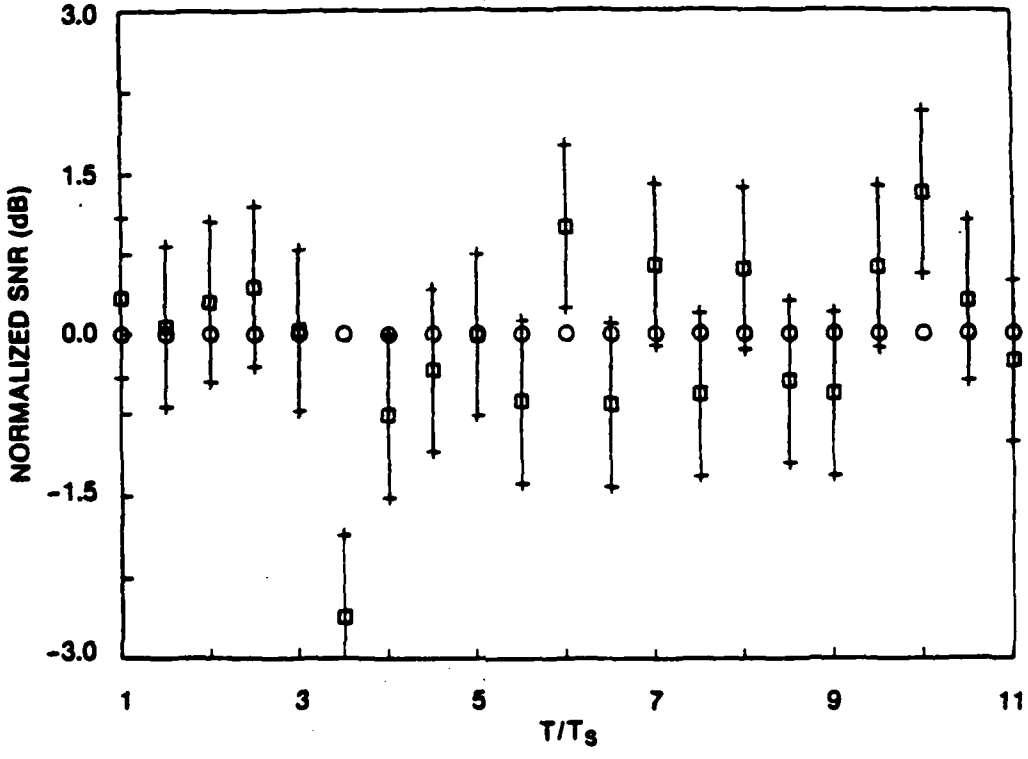

FIGURE 13. Comparison of normalized SNR for Case 8; $\sigma_{CS} = 1$, $\sigma_{HI} = 100$, $\sigma_N = 1$. Predicted values are shown as circles, simulated data shown as squares.

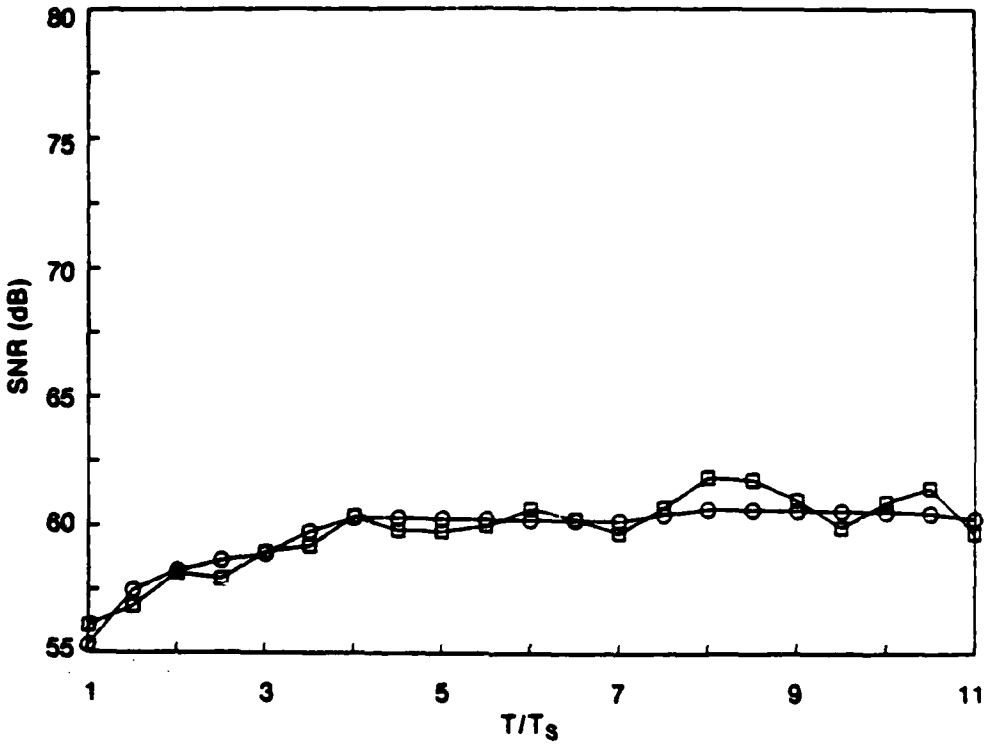

FIGURE 14. Comparison of predicted and simulated SNR for Case 7; $\sigma_{CS} = 1$, $\sigma_{HI} = 10$, $\sigma_N = 1$. Predicted values are shown as circles, simulated data shown as squares.

14, smaller reflectivity, is less dramatic than in Figure 12, larger reflectivity, with the predicted SNR increasing only 2 dB, over the continuous scatterer level. The prediction curve in Figure 14 does decrease slightly between the point scatterer returns, as expected, and jumps up at the start of the second point scatterer return. Note that the different scales between Figures 12 and 14 give the appearance that the simulation values are in Figure 14 do not follow the prediction curve as closely as the example shown in Figure 12. However, the differences between theory and model are roughly equal to the previous example, as shown in Table 2.

The normalized SNR versus T/T_s plot for this set of scattering parameters is shown in Figure 15. Four of the 19 valid simulation normalized SNR values are outside the 90 percent confidence limits, but the simulation values are more closely aligned with the normalized prediction values than the data shown in Figure 13.

4.4.2 Effects of Simulation Sample Size. All of the simulation data presented up to this point was obtained by averaging 100 simulation realizations. The differences between model and theory may be reduced by increasing the number of averages used in the comparisons. Figure 16 is a SNR versus T/T_s plot for the set of scattering parameters shown in Figure 12, but obtained using the

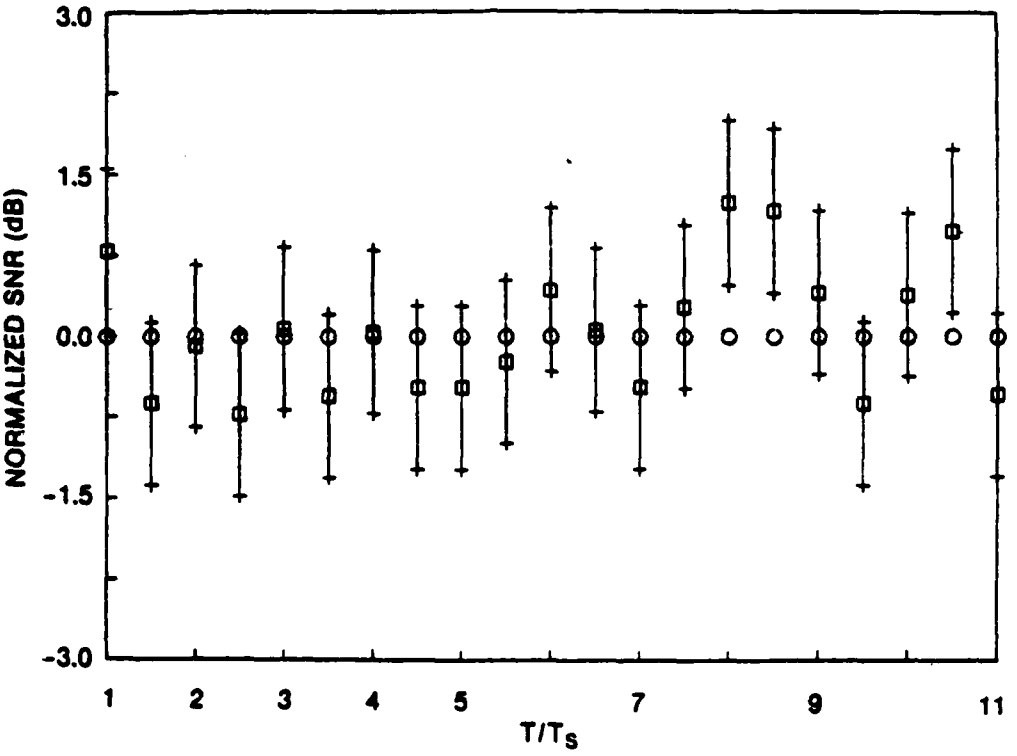

FIGURE 15. Comparison of normalized SNR for Case 7; $\sigma_{CS} = 1$, $\sigma_{HI} = 10$, $\sigma_N = 1$. Predicted values are shown as circles, simulated data shown as squares.

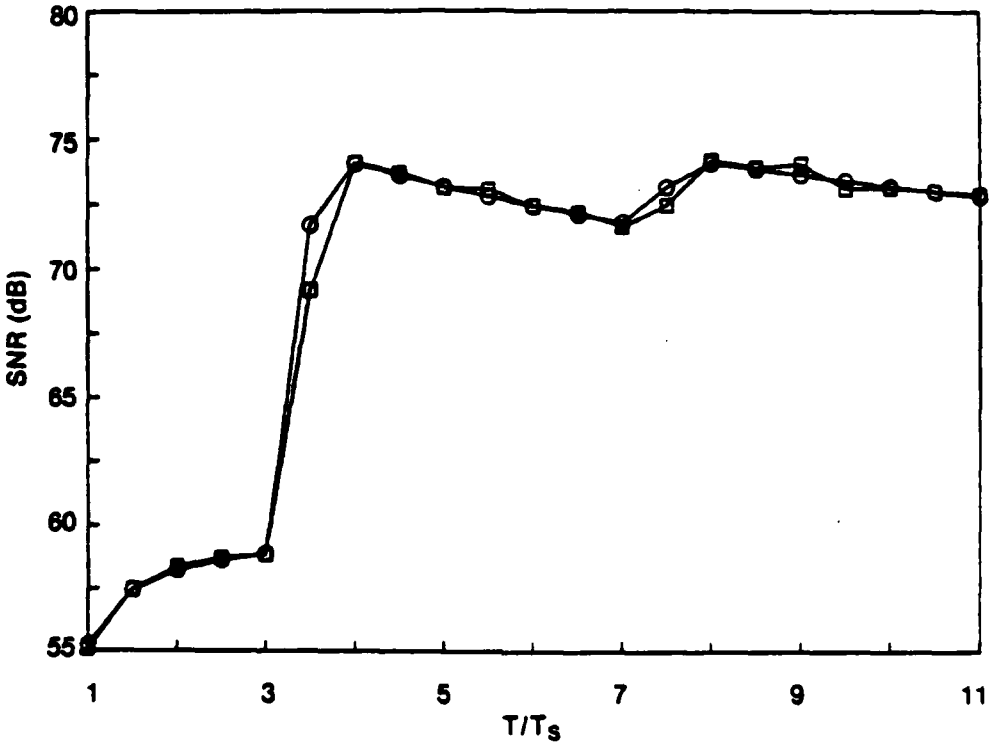

FIGURE 16. Comparison of predicted and simulated SNR for Case 8; $\sigma_{CS} = 1$, $\sigma_{HI} = 100$, $\sigma_N = 1$. Simulated SNR values obtained by averaging 1000 realizations of the scattering function. Predicted values are shown as circles, simulated data shown as squares.

average of 1000 simulation trials instead of 100. The prediction curve values are identical between this figure and Figure 12, as expected. However, the simulation values lie much more closely to the prediction curve for the 1000 trial average than for only 100 trials. The mean difference between the theory and model values in Figure 16, is only 0.2 dB, compared to 0.5 dB, for Figure 12.

The excellent agreement between the prediction equation and model is also observed in the normalized SNR versus T/T_s plot, Figure 17. Only the data point at $T/T_s = 3.5$ lies outside the 90 percent confidence limits.

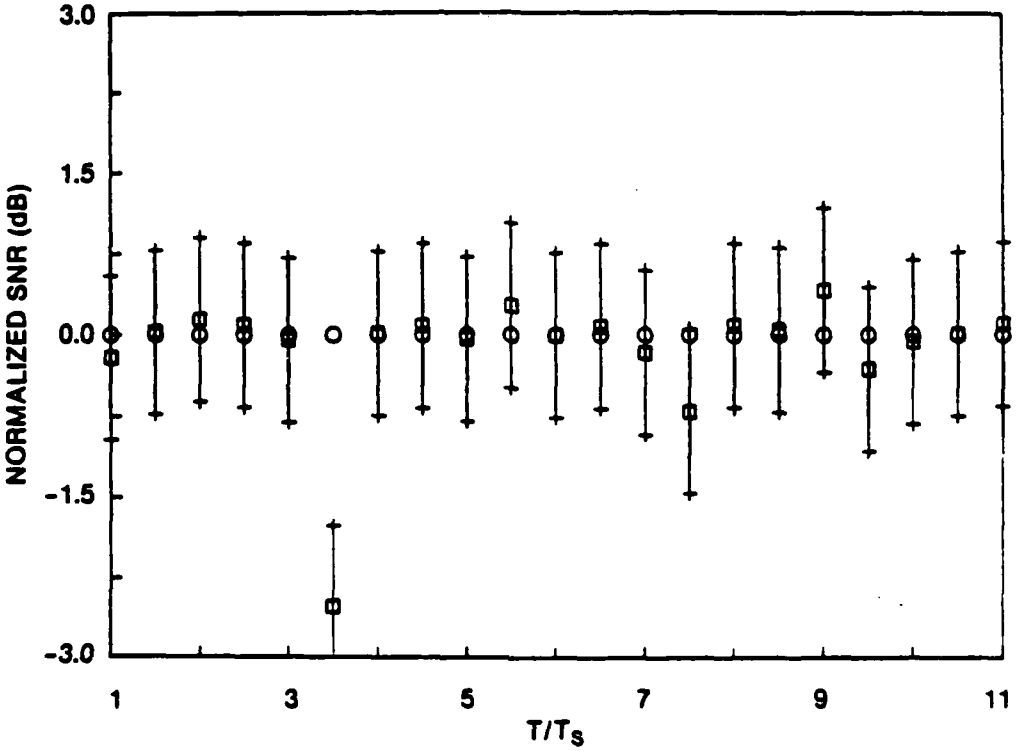

FIGURE 17. Comparison of normalized SNR for Case 8; $\sigma_{CS} = 1$, $\sigma_{HI} = 100$, $\sigma_N = 1$. Simulated SNR values obtained by averaging 1000 realizations of the scattering function. Predicted values are shown as circles, simulated data shown as squares.

CHAPTER 5

RECEIVER PERFORMANCE FOR CORRELATED CONTINUOUS SCATTER

5.1 Modifications to VanTrees' Model

5.1.1 Introduction. The model of the range spread scatterer, formulated by VanTrees, was simulated as a set of equi-spaced point reflections. The reflectivity of these point scatterers is modeled as sample functions from uncorrelated Gaussian processes. In this chapter the model is modified to allow varying degrees of interdependence, or correlation, between the individual point reflections that comprise the continuous scattering return.

This modification violates the conditions under which the scattering function is defined in Chapter 2. Indeed, for correlated scattering, the scattering function must be replaced with the more general time-frequency correlation function [18]. By comparing simulated SNR, produced using the correlated continuous scatterer, and the predicted SNR, which assumes uncorrelated scattering, the effects of correlated scattering on the validity of the prediction may be examined.

5.1.2 Simulation of the Correlated Continuous Scatterer. The assumption of uncorrelated scattering is equivalent to assuming the spectrum of the reflection process has infinite, or at least greater than half the sampling, bandwidth [19]. Correlation between the

continuous scattering components may then be achieved by low or band pass filtering the continuous scattering sequence. The degree of correlation will be inversely proportional to the filter bandwidth.

Eight filter bandwidths are used to generate varying degrees of correlation. In normalized frequency, transmit frequency divided by the sampling frequency, the normalized filter bandwidths range from 0.49, almost uncorrelated, to 0.01, almost perfectly correlated. The actual shape of the filter response is relatively unimportant, as is the difference between low and band pass. The actual filters used are based on a low pass, cosine tapered, frequency sampling filter [20]. Figures 18 and 19 are examples of the filter frequency response for normalized cutoff frequencies of 0.49 and 0.01.

To produce the correlated scattering sequence, the uncorrelated sequence is convolved with the filter impulse response. The filter output is then normalized by the ratio of the input sequence energy to the energy in the filtered sequence, producing a final, correlated scatterer, with the same total energy as the original uncorrelated sequence. This normalization insures that changes in the receiver output SNR are due solely to the correlation among the continuous scattering components.

Figures 20-24 are plots of an unfiltered sequence and the output of four filters, in decreasing bandwidth. Figure 19, generated using a filter bandwidth of 0.49 is indistinguishable from the unfiltered

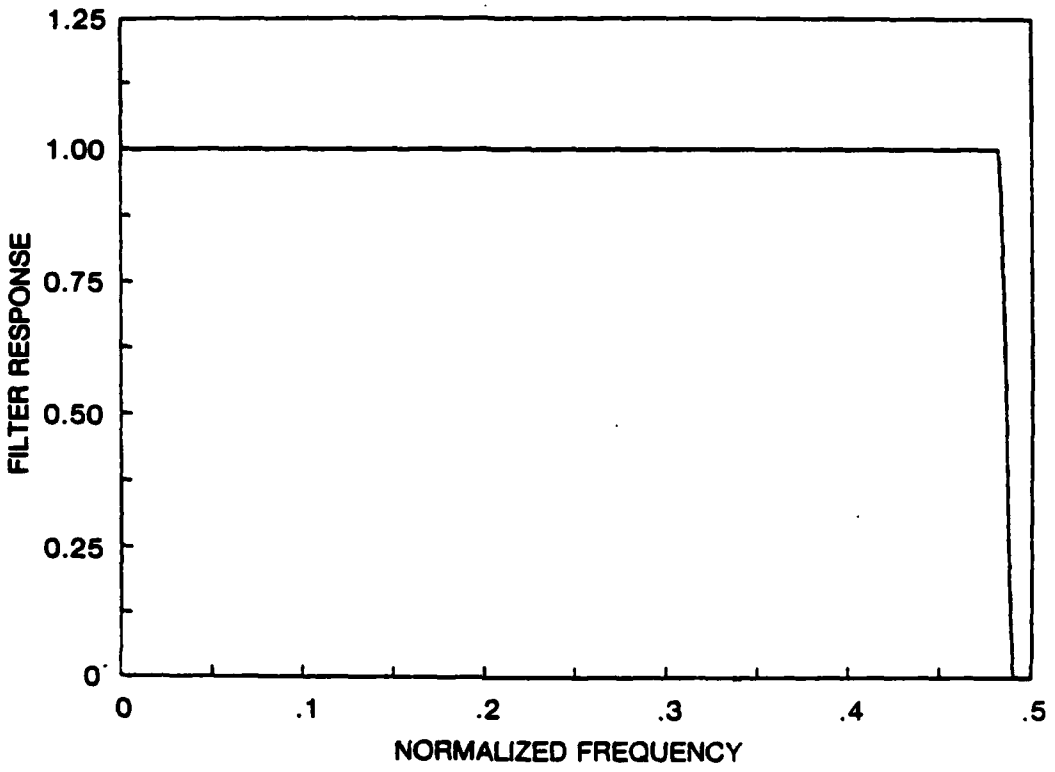

FIGURE 18. Frequency response of filter used to generate the correlated scattering sequence. The filter bandwidth is 0.49.

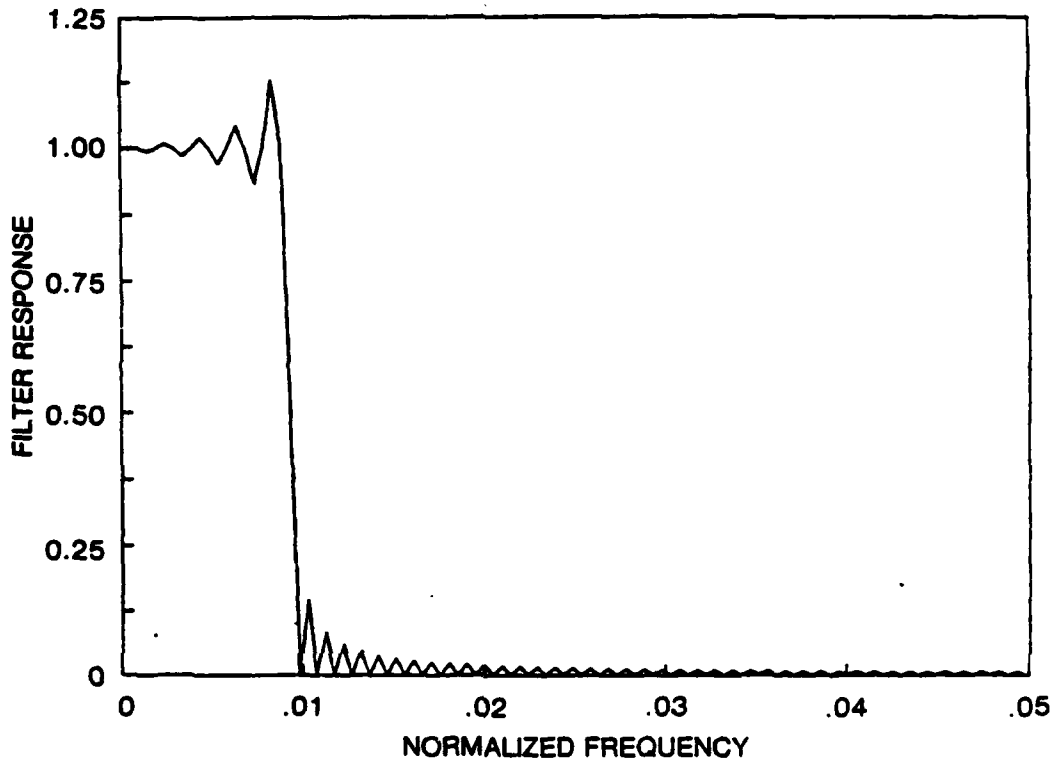

FIGURE 19. Frequency response of filter used to generate the correlated scattering sequence. The filter bandwidth is 0.01.

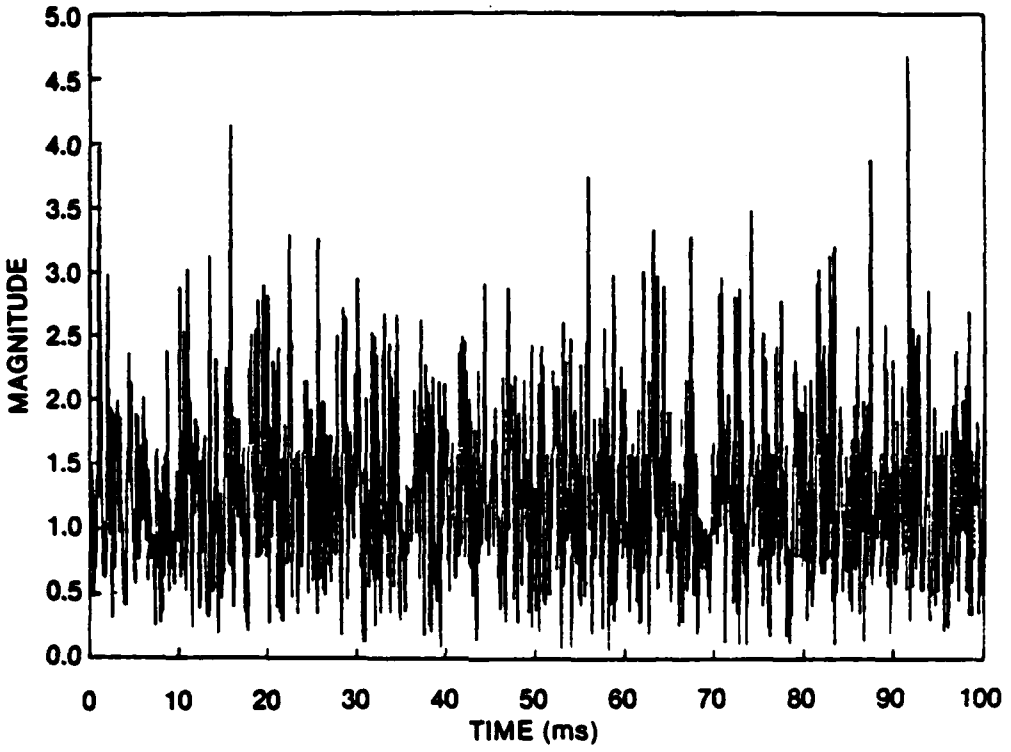

FIGURE 20. Uncorrelated scattering sequence. Sequence energy = 65.95 dB.

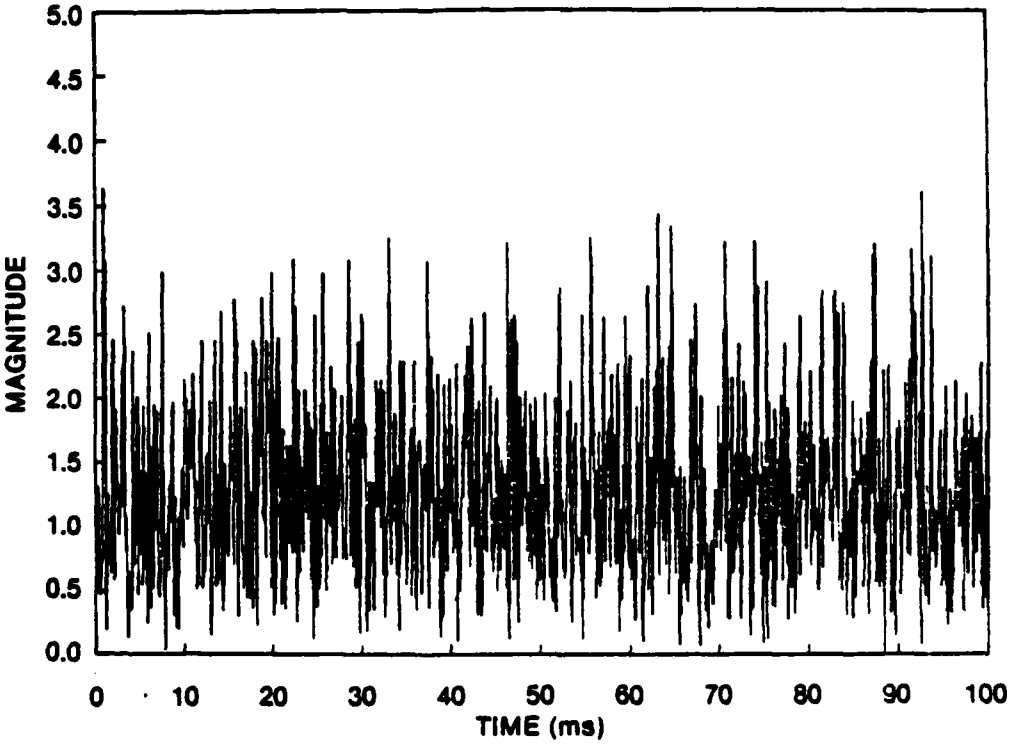

FIGURE 21. Correlated scattering sequence for a filter bandwidth of 0.49. Sequence energy = 65.95 dB.

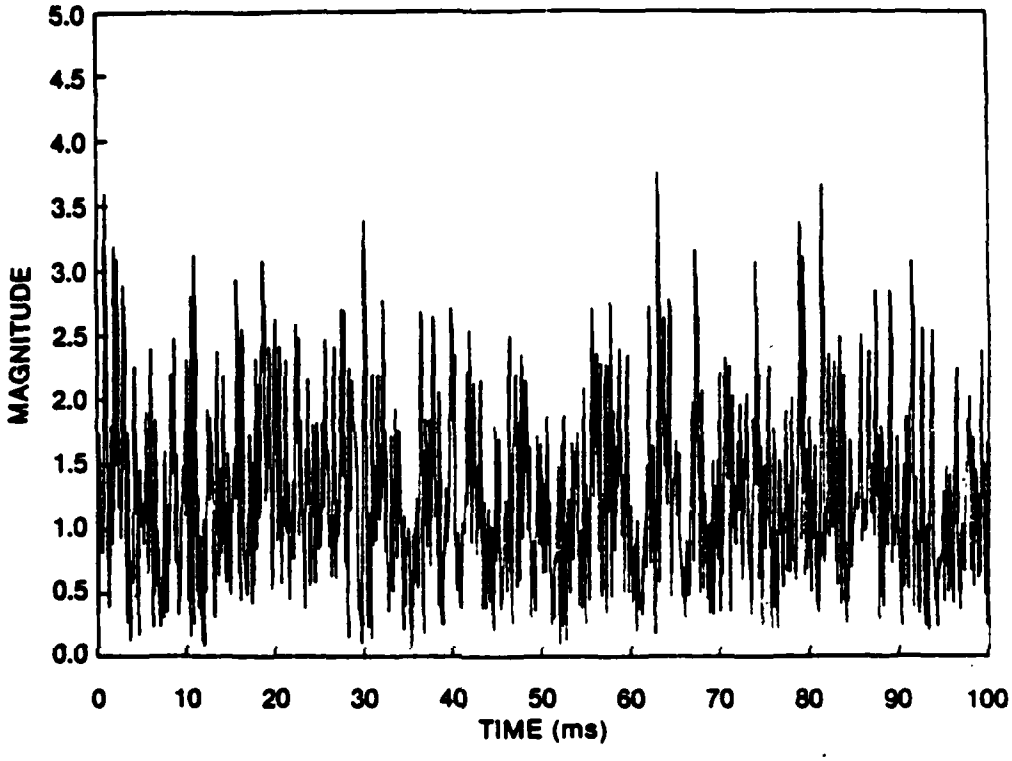

FIGURE 22. Correlated scattering sequence for a filter bandwidth of 0.25. Sequence energy = 65.95 dB.

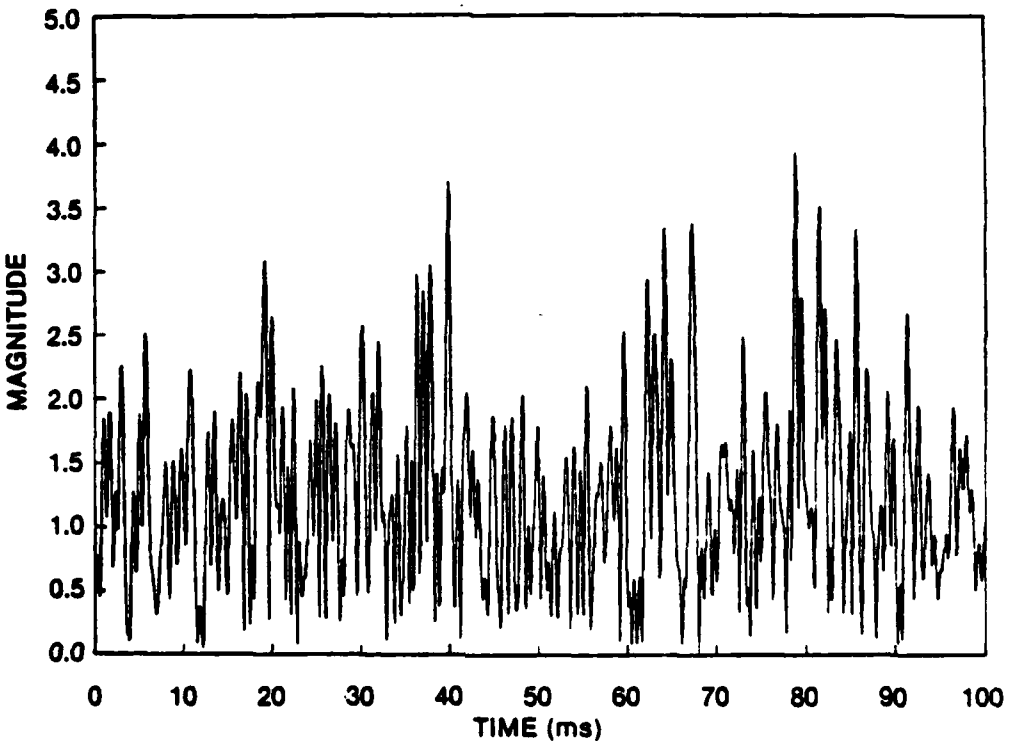

FIGURE 23. Correlated scattering sequence for a filter bandwidth of 0.1. Sequence energy = 65.95 dB.

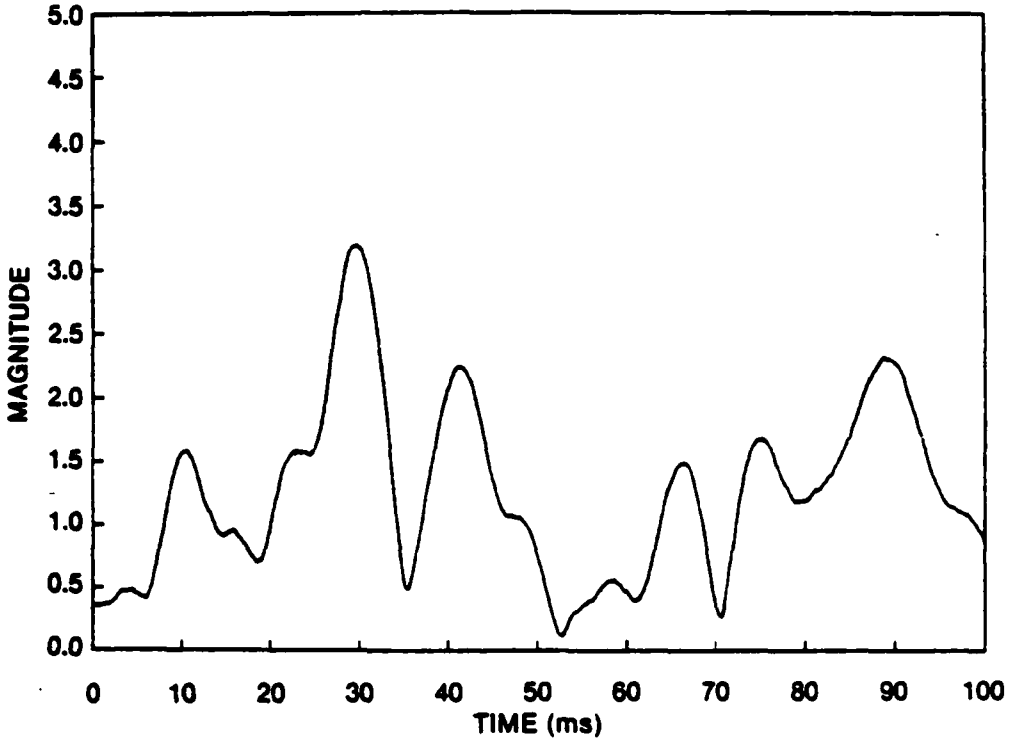

FIGURE 24. Correlated scattering sequence for a filter bandwidth of 0.01. Sequence energy = 65.95 dB.

data. As the bandwidth shrinks, the sequence appears more sinusoidal than random, as expected. Note the energy of each sequence in Figures 20-24 is identical, 65-95 dB. To generate the correlated composite scatterer, the two point reflectors are then added to the filtered continuous scattering sequence at samples 300 and 700, as discussed previously.

5.2 Correlated Continuous Scatterer Results

5.2.1 SNR Comparison versus Bandwidth. Table 3 lists the comparison statistics for the correlated scatterer simulation and predicted uncorrelated SNR. The related figures are 25-29. As with the uncorrelated continuous scatterer data, comparisons between the simulated and predicted SNR values, do not include data at T/T_s = 3.0 and 3.5.

In Figure 25, the filter bandwidth is large, and the comparison between simulation and prediction is quite good. Indeed, the statistical comparison for this data set is as good as any uncorrelated data comparison. The quality of the comparison is also seen in the normalized comparison, Figure 26. Note the majority of the prediction values fall within the 90 percent confidence interval; only the values at T/T_s = 5.5 and 7.0 are outside this range. The average difference between simulation and prediction is 1.1 dB, comparable to all the uncorrelated scattering data.

TABLE 3 - Scattering Strength Parameters and Statistics of Differences between Simulated and Predicted and Simulated Signal-to-Noise Ratios Assuming Correlated Continuous Scattering.

CASE NO.	BW	STANDARD DEVIATION OF SCATTERING MODEL PARAMETERS σ_{CS}	σ_{HI}	σ_N	DIFFERENCES BETWEEN MODEL AND THEORY (Average of all values of T/T_S.) MAX DB	MEAN DB	ST. DEV. DB
15	0.49	1.	0.	1.	1.1	0.4	0.3
23	0.40	1.	0.	1.	2.5	1.2	0.6
16	0.25	1.	0.	1.	4.3	3.2	0.6
24	0.15	1.	0.	1.	6.8	5.5	0.6
17	0.10	1.	0.	1.	8.2	7.1	0.6
25	0.05	1.	0.	1.	11.0	10.1	0.5
26	0.02	1.	0.	1.	15.2	14.1	0.6
18	0.01	1.	0.	1.	18.2	17.3	0.6
19	0.49	1.	100.	1.	1.3	0.4	0.3
20	0.25	1.	100.	1.	4.3	1.1	1.1
21	0.10	1.	100.	1.	7.6	1.9	2.6
22	0.01	1.	100.	1.	17.3	7.5	4.7

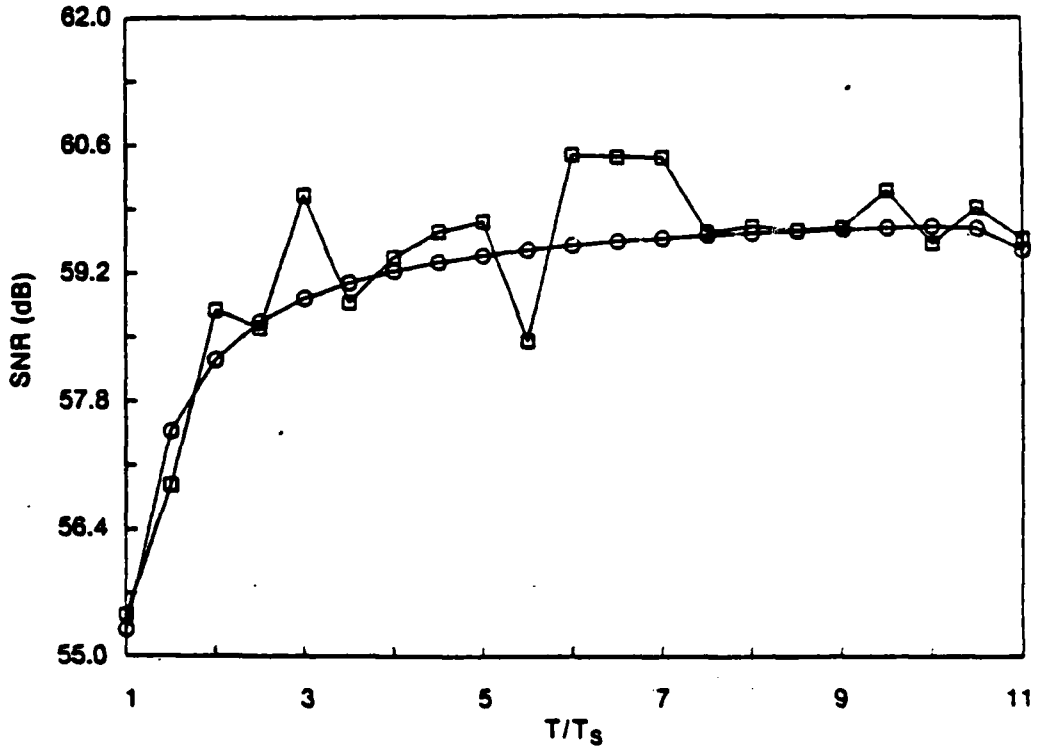

FIGURE 25. Comparison of uncorrelated continuous scattering SNR prediction, and correlated scattering simulation for Case 15; $\sigma_{CS} = 1$, $\sigma_{HI} = 0$, $\sigma_N = 1$, filter bandwidth = 0.49. Predicted values are shown as circles, simulated data shown as squares.

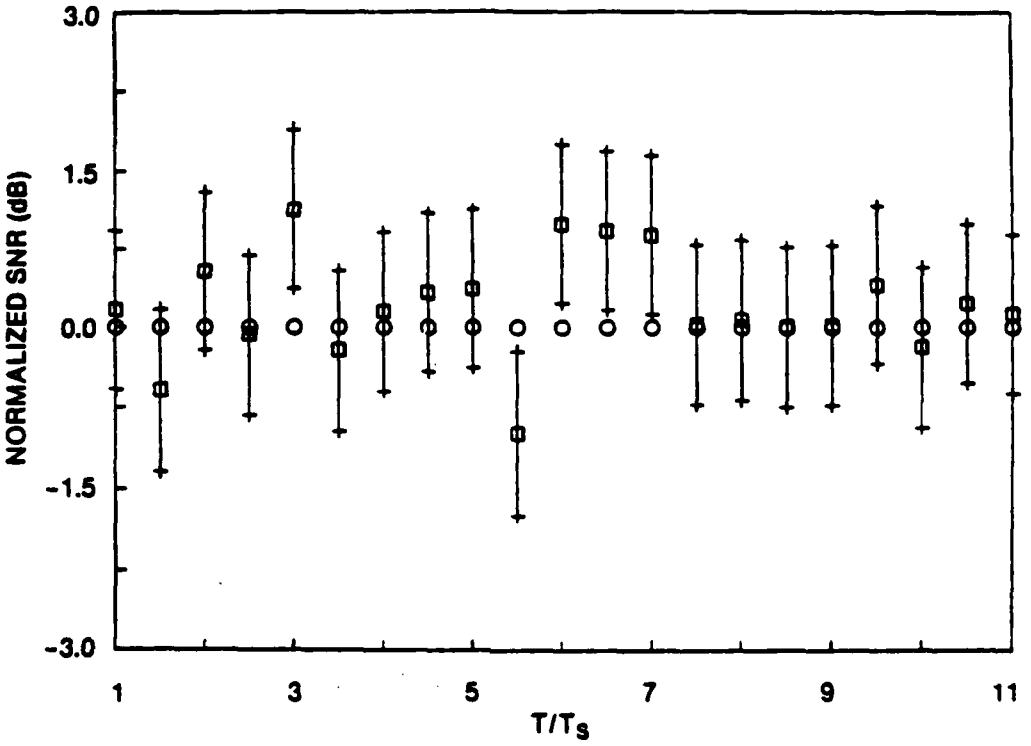

FIGURE 26. Comparison of normalized uncorrelated continuous scattering SNR prediction, and correlated scattering simulation for Case 15; $\sigma_{CS} = 1$, $\sigma_{HI} = 0$, $\sigma_N = 1$, filter bandwidth = 0.49. Predicted values are shown as circles, simulated data shown as squares.

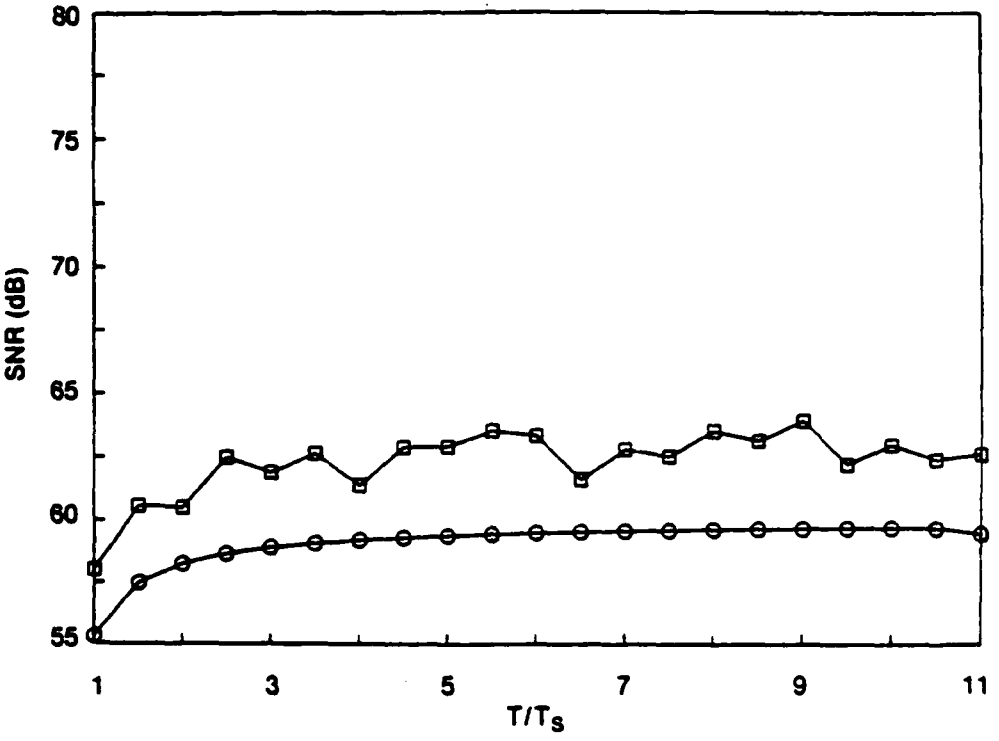

FIGURE 27. Comparison of uncorrelated continuous scattering SNR prediction, and correlated scattering simulation for Case 16; $\sigma_{CS} = 1$, $\sigma_{HI} = 0$, $\sigma_N = 1$, filter bandwidth = 0.25. Predicted values are shown as circles, simulated data shown as squares.

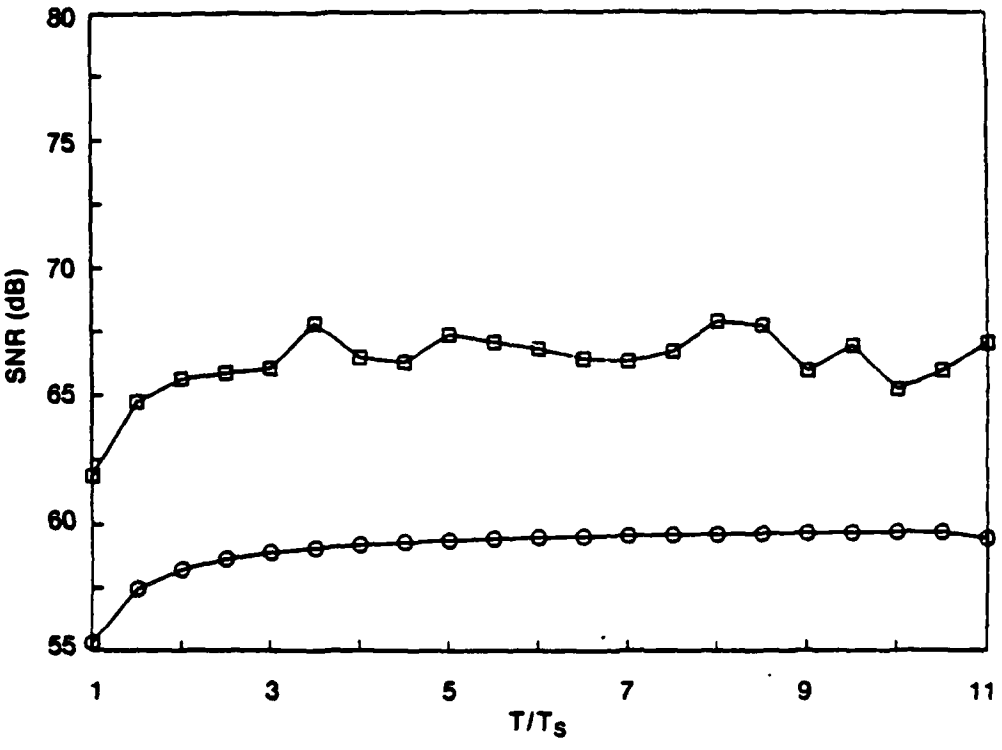

FIGURE 28. Comparison of uncorrelated continuous scattering SNR prediction, and correlated scattering simulation for Case 17; $\sigma_{CS} = 1$, $\sigma_{HI} = 0$, $\sigma_N = 1$, filter bandwidth = 0.1. Predicted values are shown as circles, simulated data shown as squares.

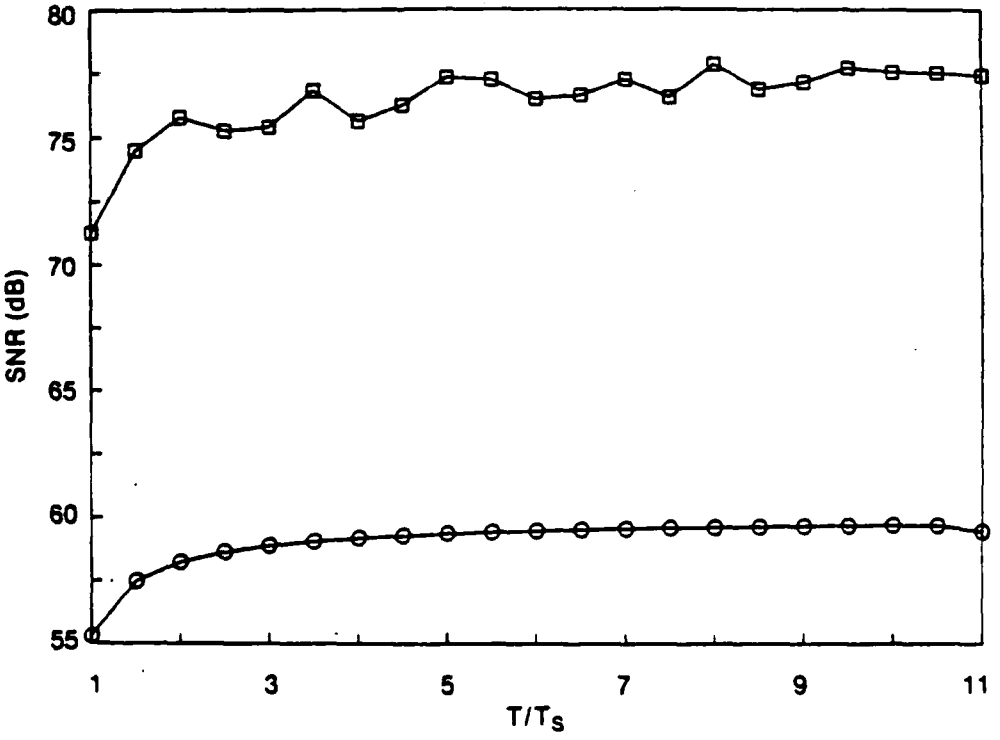

FIGURE 29. Comparison of uncorrelated continuous scattering SNR prediction, and correlated scattering simulation for Case 18; $\sigma_{CS} = 1$, $\sigma_{HI} = 0$, $\sigma_N = 1$, filter bandwidth = 0.01. Predicted values are shown as circles, simulated data shown as squares.

In Figure 27, the filter bandwidth is reduced to 0.25, and the simulated SNR shows a 3 dB gain at all values of T/T_s over the predicted SNR. However, the slope of the two curves are similar, and as indicated by the relatively small standard deviation associated with the simulation data, and the correlated scattering results display no more variation on a point-to-point basis than the uncorrelated scattering simulations. No normalized data is presented since for this bandwidth, all the predicted values fall well outside the uncorrelated confidence intervals.

For a bandwidth of 0.1, Figure 28, the mean SNR difference has increased to 7 dB, but the shape of the correlated scattering data curve is similar to the prediction curve. In addition, the variation of the simulated data about the mean offset is comparable to uncorrelated scattering data.

The 0.01 filter bandwidth, highly correlated data, shown in Figure 29, has a similarly small variation, but the mean offset is greater than 17 dB, and independent of T/T_s. If there was some dependence on the absolute value to T/T_s, we might expect a linear gain in SNR with increasing T. This behavior would increase the standard deviation of the SNR, but the values listed in Table 3 appear to be equal to the uncorrelated scattering data.

5.2.2 Corrections for Correlated Scattering. The SNR comparisons in Figures 25-29 suggest a correction factor might be applied to the uncorrelated prediction to account for the presence of correlated scattering. Two different types of curve fits are employed. The first is suggested by the simulation data, and assumes the correction equation is of the form,

$$\text{SNR Gain (dB)} = e^{\alpha(0.5-f)} \qquad (5.1)$$

where SNR Gain is the mean difference between the predicted SNR values and correlated simulation SNR; f is the normalized filter bandwidth, and it is assumed the SNR Gain at 0.5 is zero. Several values of the coefficient a were plotted to obtain a empirical best fit. Figure 30 is a plot of the SNR Gain versus filter bandwidth for the eight cases examined. Also plotted are three realizations of Equation 5.1, with values of α = 5.6, 5.8 and 5.9. All three curves provide a reasonable fit for frequencies greater than 0.25. At frequencies less than 0.25, all the the fitted curves predict too large a SNR Gain, by 1-2 dB. For very small filter bandwidths, the gain indicated by the data appears to increase much faster than any of the fits provided by Equation 5.1.

A second fit to the data is a simple polynomial fit. For only 8 data points, the degree of the fitted polynomial is restricted to between 2 and 4. Table 4 lists the coefficients computed by the IMSL routines RLFOTH and RLDOPH for the three orders examined [21]. A plot

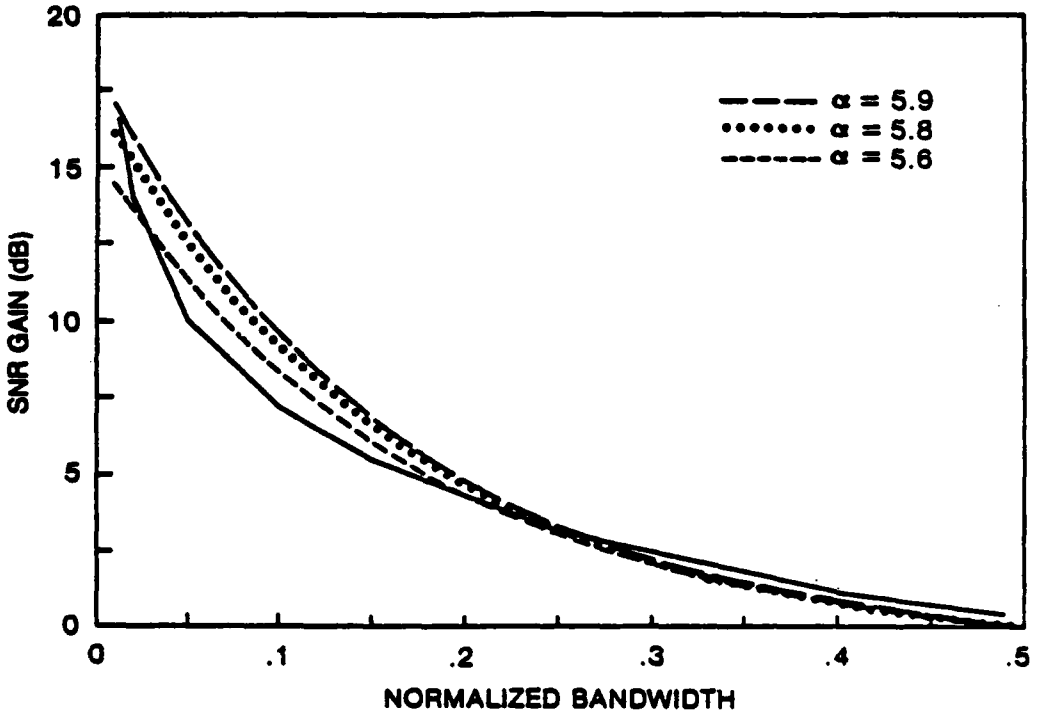

FIGURE 30. Exponential fit to SNR gain versus filter bandwidth for α = 5.6, 5.8 and 5.9. SNR gain obtained from simulation is shown as the solid line.

TABLE 4 - Coefficients of Polynomials Fitted to Continuous Correlated Scatterer SNR Gain versus Filter Bandwidth Data (See Figure 33).

POLYNOMIAL DEGREE	A0	A1	A2	A3	A4
2	15.7	-80.9	105.1		
3	17.2	-132.8	401.4	-411.3	
4	18.3	-194.5	1025.5	-2434.8	2041.9

of the data with the three fitted polynomials is shown in Figure 31. Clearly, the accuracy of the fit increases with increasing polynomial degree, though each increase in order adds an additional inflection point not indicated by the data.

Figure 32 plots the best mean square fit for both models and the SNR Gain data. The quality of the polynomial fit is clearly better than the exponential model, particularly in the frequency range from 0.2 to 0.05 Hz. The fourth order polynomial equation appears to be the most accurate fit to the correlated scattering gain, and might be used with the uncorrelated scattering prediction to estimate the correlation of an actual scattering process.

5.3 Composite Correlated Scatterer SNR Comparison

Four cases examine the correlated continuous scatterer with two large amplitude, point reflectors. Table 3 lists the simulation and uncorrelated scattering prediction comparison statistics, for constant scattering strength parameters and increasing degrees of continuous scatterer correlation. The related figures are 33-38.

In Figure 33, for a filter bandwidth of 0.49, the comparison between simulated and predicted signal-to-noise ratios is quite good. As with the uncorrelated scatterer data, the greatest difference between simulation and prediction occurs at $T/T_s = 3.5$, an indication that the SNR is dominated by the point scatterers returns

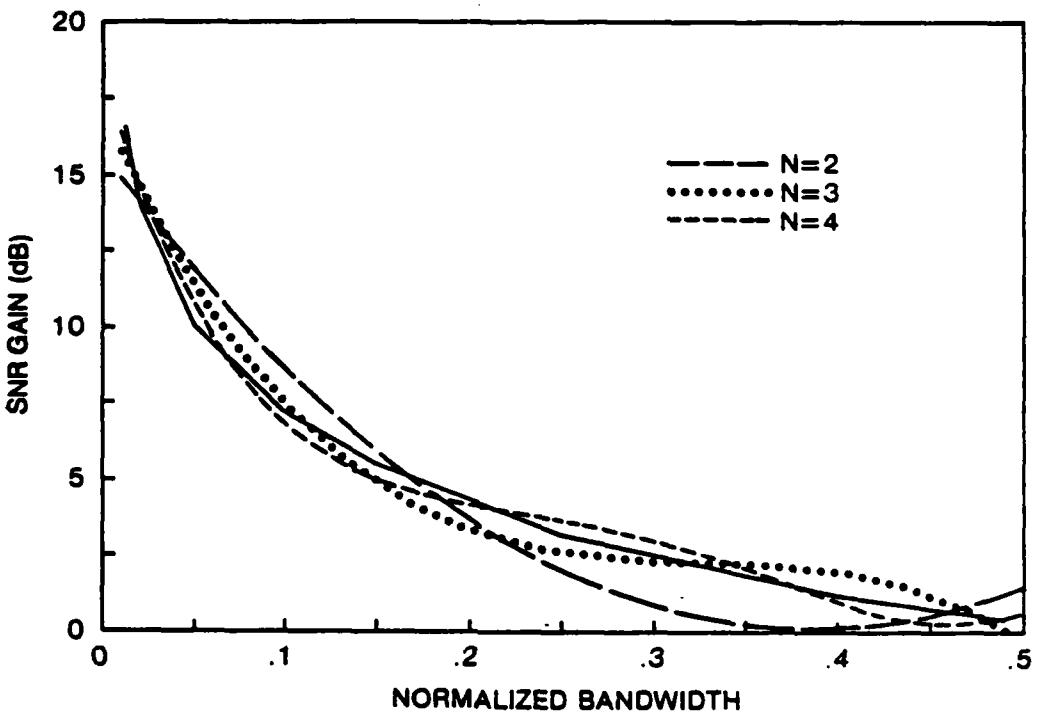

FIGURE 31. Polynomial fit to SNR gain versus filter bandwidth for polynomial orders, N, = 2, 3 and 4. True SNR gain shown as solid line.

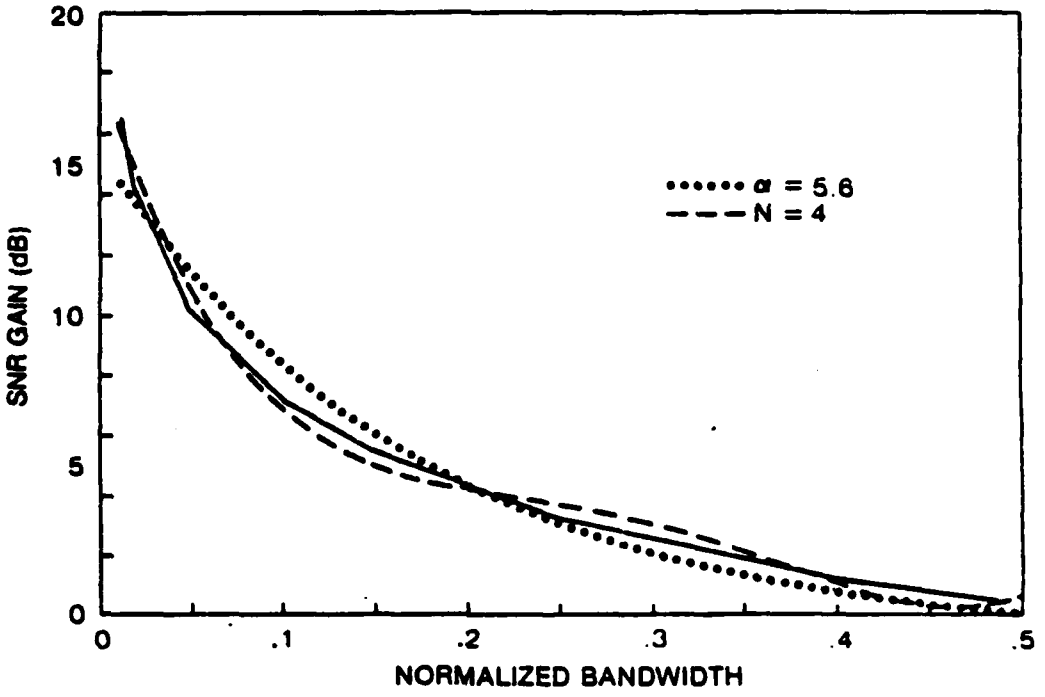

FIGURE 32. Best fits for polynomial and exponential models to SNR gain versus filter bandwidth. True SNR gain shown as solid line.

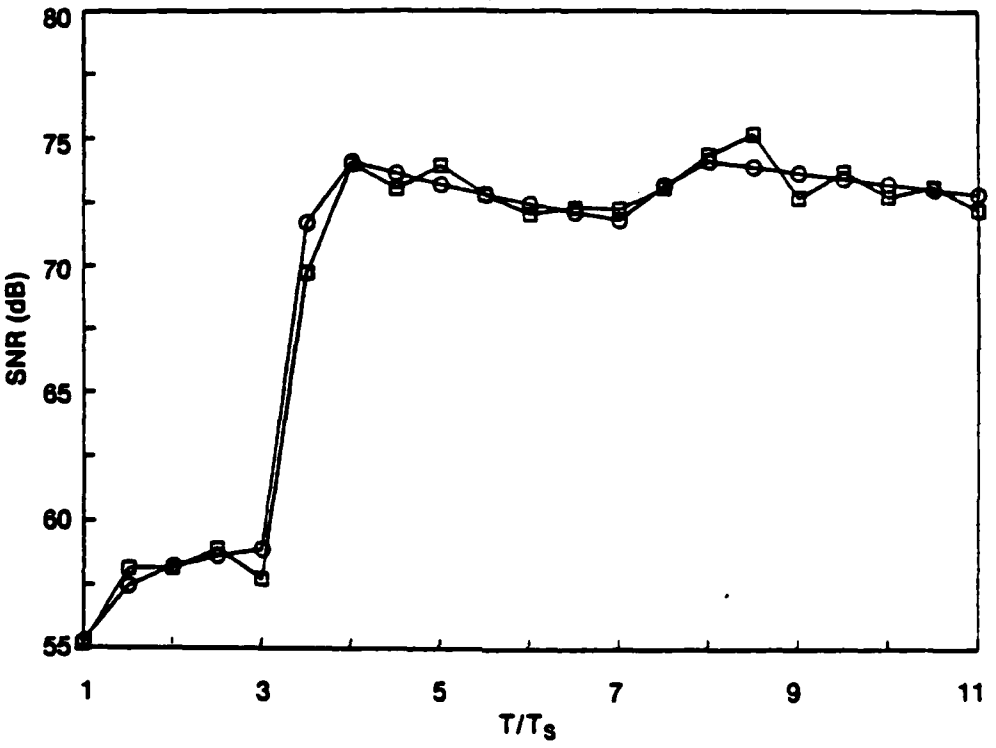

FIGURE 33. Comparison of uncorrelated continuous scattering SNR prediction, and correlated scattering simulation for Case 19; $\sigma_{CS} = 1$, $\sigma_{HI} = 100$, $\sigma_N = 1$, filter bandwidth = 0.49. Predicted values are shown as circles, simulated data shown as squares.

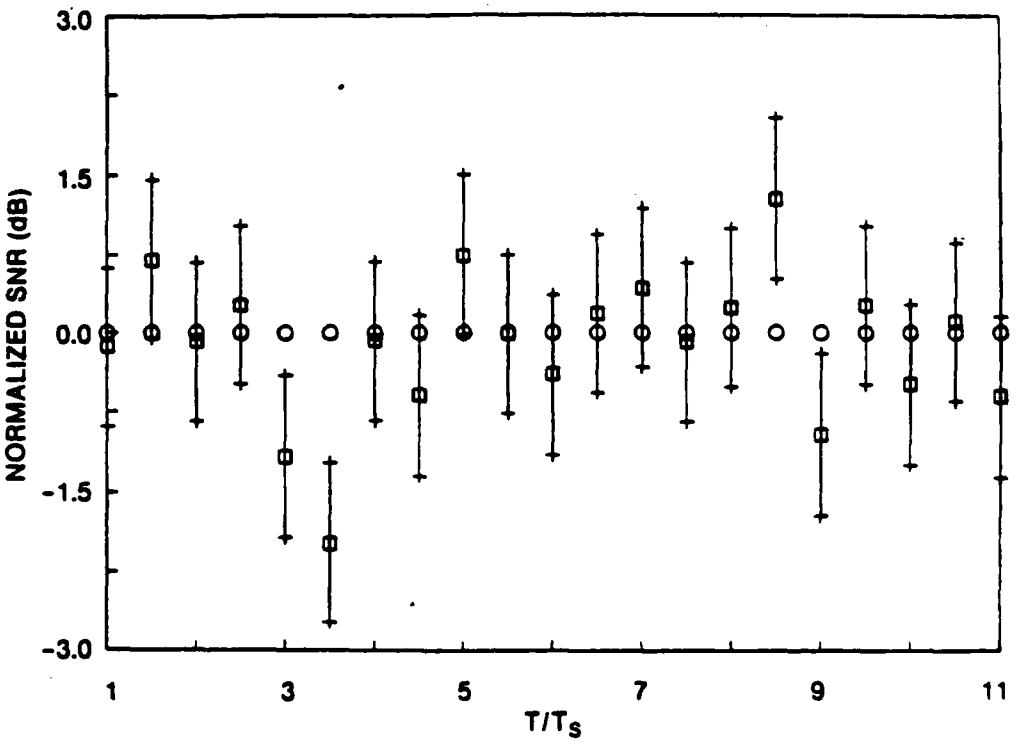

FIGURE 34. Comparison of normalized uncorrelated continuous scattering SNR prediction, and correlated scattering simulation for Case 19; $\sigma_{CS} = 1$, $\sigma_{HI} = 100$, $\sigma_N = 1$, filter bandwidth = 0.49. Predicted values are shown as circles, simulated data shown as squares.

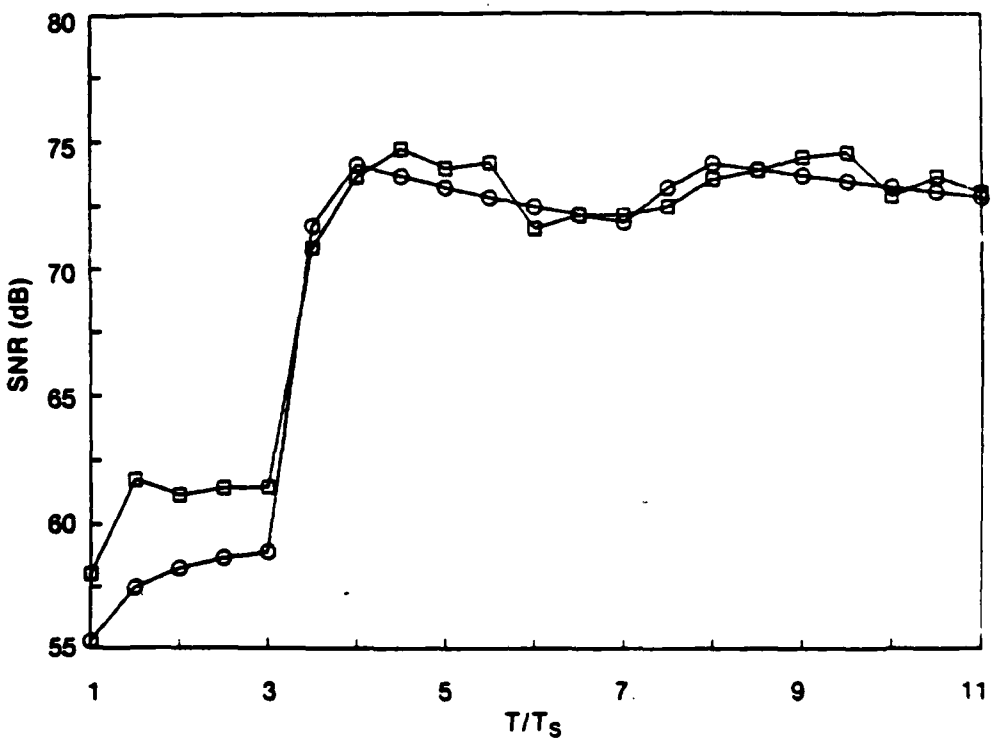

FIGURE 35. Comparison of uncorrelated continuous scattering SNR prediction, and correlated scattering simulation for Case 20; $\sigma_{CS} = 1$, $\sigma_{HI} = 100$, $\sigma_N = 1$, filter bandwidth = 0.25. Predicted values are shown as circles, simulated data shown as squares.

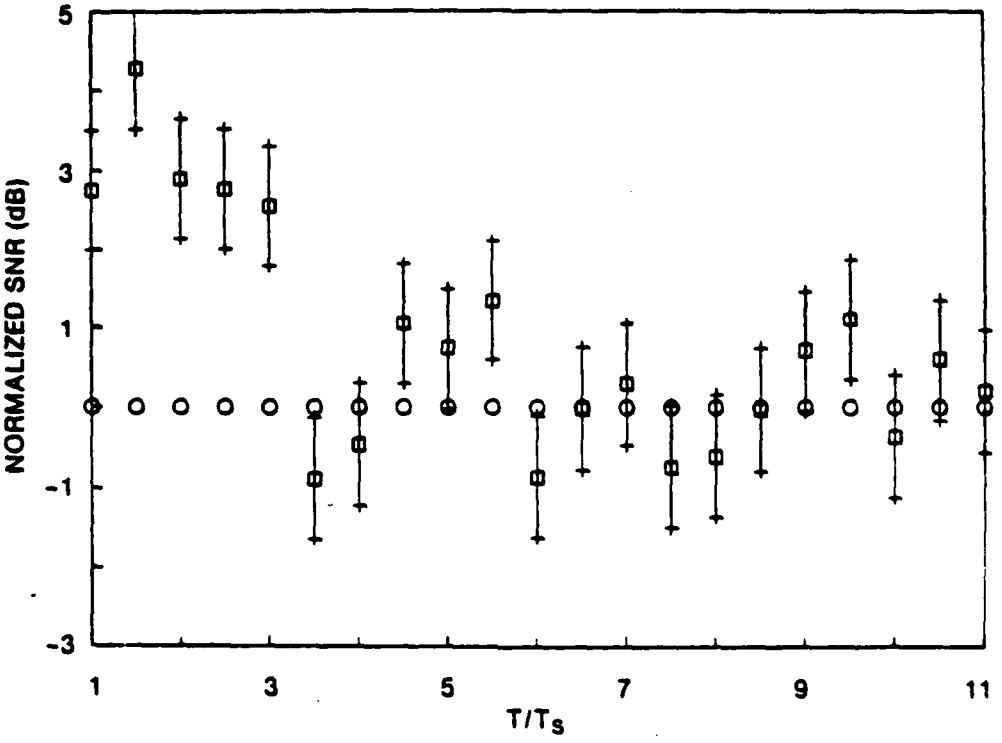

FIGURE 36. Comparison of normalized uncorrelated continuous scattering SNR prediction, and correlated scattering simulation for Case 20; $\sigma_{CS} = 1$, $\sigma_{HI} = 100$, $\sigma_N = 1$, filter bandwidth = 0.25. Predicted values are shown as circles, simulated data shown as squares.

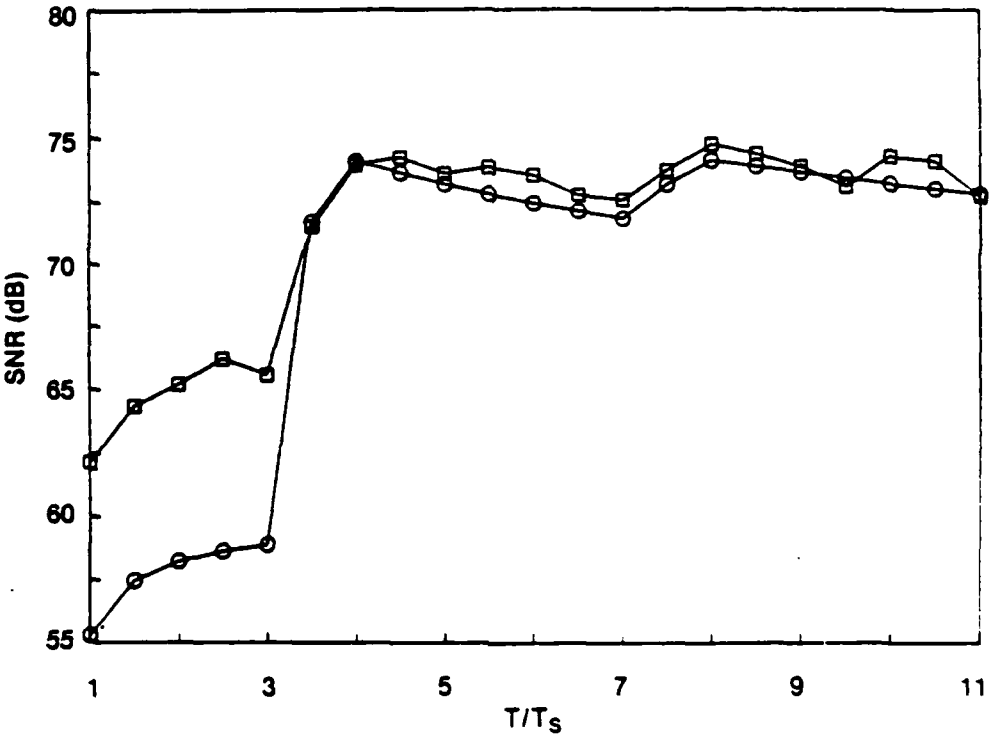

FIGURE 37. Comparison of uncorrelated continuous scattering SNR prediction, and correlated scattering simulation for Case 21; $\sigma_{CS} = 1$, $\sigma_{HI} = 100$, $\sigma_N = 1$, filter bandwidth = 0.10. Predicted values are shown as circles, simulated data shown as squares.

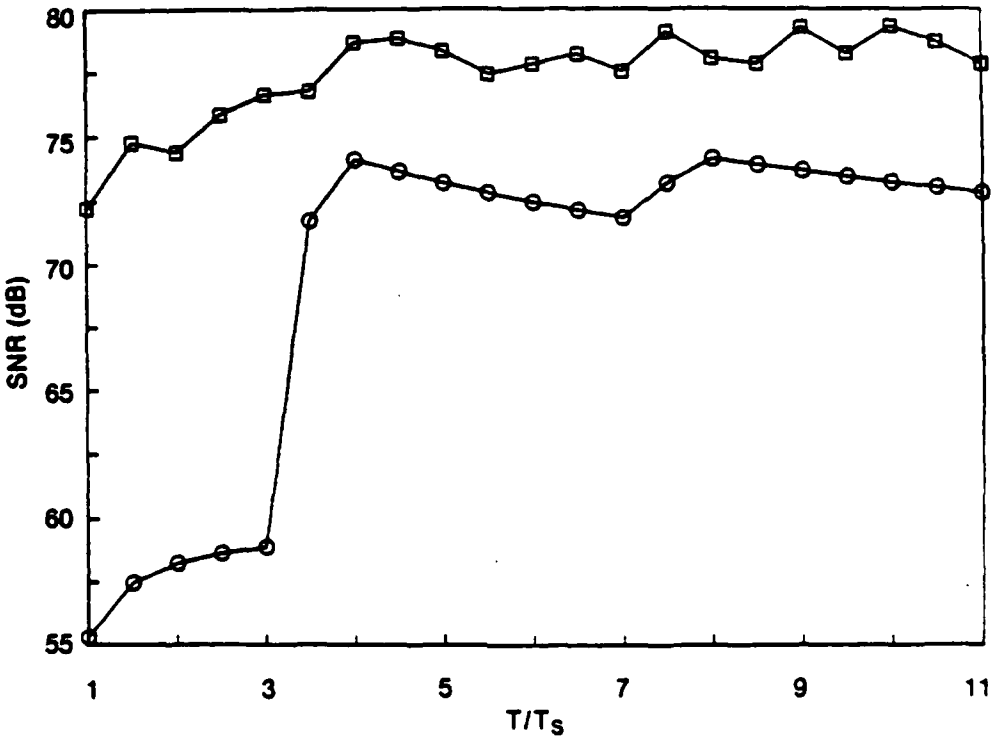

FIGURE 38. Comparison of uncorrelated continuous scattering SNR prediction, and correlated scattering simulation for Case 22; $\sigma_{CS} = 1$, $\sigma_{HI} = 100$, $\sigma_N = 1$, filter bandwidth = 0.01. Predicted values are shown as circles, simulated data shown as squares.

after T/T_s = 3.0. For this case, any offset introduced by the correlated continuous scatterer is smaller than the variation of the uncorrelated scatter. The normalized SNR comparison, Figure 33, also indicates the quality of the SNR comparison is good. The only points that lies outside the 90 percent confidence interval are associated with the two point scatterer returns.

Figure 35 shows the SNR comparison for a normalized filter bandwidth of 0.25. The comparison of simulation and prediction prior to the first point scatterer return shows that the correlated scattering levels are 3-4 dB greater than the predicted uncorrelated values, with the greatest difference 4.3 dB, at T/T_s = 1.5. Beyond the first point scatterer return, the comparison between simulated and predicted levels appears to be reasonably good. The added energy due to the correlated scattering levels is still 10 dB below the SNR produced with the point scatterers returns, and therefore does not appear to significantly add to the overall SNR.

The effects of the correlated scatter for this filter bandwidth also appear in Figure 36, normalized SNR versus T/T_s. The data prior to the point reflection return at T/T_s = 3.0 is roughly 3 dB above the predicted levels, and well outside the 90 percent confidence interval. The data after the first point scatterer return displays

AD-A173 355 PERFORMANCE OF MISMATCHED RECEIVERS AGAINST RANGE SPREAD SCATTERERS(U) NAVAL UNDERWATER SYSTEMS CENTER NEWPORT RI W S HAUCK 19 SEP 86 NUSC-TR-7779 2/2

UNCLASSIFIED F/G 9/4 NL

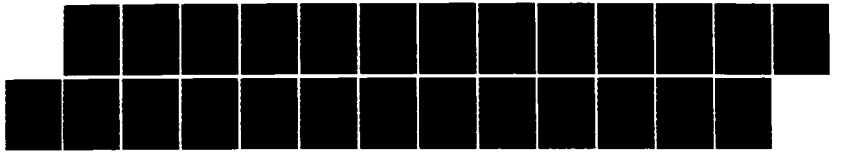

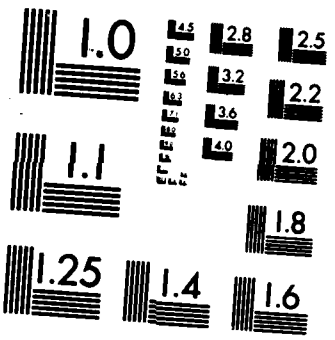

more point to point variation than previous data sets, but no systematic error is apparent. If the correlated scatterer affected this portion of the data, a similar, but smaller positive offset of the data might be expected. Since this is not evident, it appears the gain due to correlated scattering is still insignificant compared to the point reflector returns.

For a filter bandwidth of 0.1, Figure 37, the simulated correlated scattering values prior to the first highlight return are roughly 7 dB higher than predicted levels. Beyond the start of the first point scatterer return, the SNR comparison is still good, but the simulated data shows a slight, ~0.5 dB, positive bias.

The comparison for a narrow filter bandwidth, 0.01, is shown in Figure 38. The simulated level prior to the first point scatterer reflection are greater than the predicted levels including the point scatterer returns. As a result, the correlated continuous scattering is the dominate scattering process at all values of T/T_s. Note the simulated SNR curve rises only 4-5 dB after the point scattering returns, an indication that the correlated scattering and highlight scattering energies are roughly equivalent. The SNR gain prior to the point scatterers is roughly 17 dB, as listed in Table 3.

CHAPTER 6

CONCLUSIONS

6.1 Summary and Conclusions

6.1.1 Models. In this thesis, results for an analytic model and computer simulation have been compared under a variety of conditions. The model assumes that a transmit pulse of duration T_s propagates through a lossless isotropic medium and is reflected from a randomly rough, range spread scatterer. The scatterer is modeled as the sum of two components. The first is a continuous line scatterer, and the second, two large amplitude point reflectors, whose locations are fixed along the length of the continuous scatterer. The reflected signal is the convolution of the transmit pulse and a random scatterer whose average reflection characteristics are described by the target scattering function, plus white, Gaussian noise.

The signal is processed using a complex crosscorrelation receiver, and the output is examined as a function of increasing receiver integration time, T. Integration times from $T/T_s = 1.0$, integration time equal to a transmit pulse length, to $T/T_s = 11.5$, a time that is slightly greater than the duration of the reflected signal are examined. By assuming closed-form expressions for the scattering function and transmit and receiver processing waveforms, the output of the receiver may be expressed in terms of the scattering function and the receiver crossambiguity function. The mean receiver

output is written in terms of the variances of the various target components and the ratio T/T_s, predicting the receiver output signal energy to noise energy ratio.

6.1.2 Simulation. These models are simulated on a computer to test the validity of the SNR prediction equation. The continuous scatterer is simulated as a set of equi-spaced, uncorrelated, complex, Gaussian, point reflectors, each of zero mean and equal variance. This model is taken from VanTrees for a range spread scattering function. The point scatterer model is the slowly fluctuating point target, also from VanTrees. The point reflectors are simulated as two uncorrelated, complex, Gaussian numbers, whose variance is large compared to the variance of the continuous scattering components. The average output of the correlation receiver is computed by averaging 100 realizations of the signal and passing it through the receiver, and separately 100 noise sequences, for constant scattering strength parameters. These two results are then divided to obtain the statistic to compare with the prediction equation.

6.1.3 Results and Errors. Agreement between simulation and prediction is quite good, with the mean error less than 0.5 dB. The quality of agreement is independent of the absolute SNR, the relative scattering strengths of the scattering components, and is generally independent of the receiver integration time. It is apparent from these comparisons that the prediction equation accurately predicts the receiver output for all the scattering strength and T/T_s ratios

examined. This further validates the analysis of the model using scattering and ambiguity functions, allowing this technique to be extended to more complex scatterers and waveforms. However, two types of disagreement were identified, and can be traced to either a transition between the dominate scattering components or to the effects of averaging over a finite set of simulation values.

The first type of comparison difference occurs at receiver integration times that include the onset of the first highlight reflection. These times, at values of T/T_s = 3.0 and 3.5 correspond to processing the reflected signal on the start of the first point scatterer reflection. For T/T_s = 3.0, only a single sample of the large amplitude reflection is included with the continuous scattering return. For T/T_s = 3.5, half the first point scattering return is included. The comparison difference for data at T/T_s = 3.5 is generally 2-3 dB greater than the overall mean comparison difference. Since a small number of large values are being averages, when compared to either greater or smaller values of T/T_s are averaged, it is expected that the variance in the estimate will be greater. This behavior is not seen in the comparison at T/T_s = 3.0 because the energy in the single point scatterer sample included by the receiver is small compared to the energy in the 300 continuous scattering samples, and does not effect the estimate of signal energy, as does 50 samples for T/T_s = 3.5.

An independent confirmation of this conclusion comes by increasing the number of model realizations averaged to obtain the simulation comparison value. While this is cost prohibitive for all combinations of scatterers and receiver integration times, comparisons of 1000 and 10000 averages show the comparison error at $T/T_s = 3.5$ declines dramatically. Indeed, for large numbers of signals in the average, all the simulation data approaches the predicted values. It is concluded that the differences seen between simulation and prediction outside the region near $T/T_s = 3.0$, the second type of error observed, can be reduced by increasing the number of model realizations used to compute the average signal and noise energies.

6.1.4 Correlated Scattering. A modification of the continuous scattering model was made by filtering the continuous scattering sequence to produce a sequence with correlation between the continuous scattering components. The scattered signal is processed as described above, and the averaged result compared to the prediction for uncorrelated scattering.

For the correlated continuous scatterer only, the quality of the comparison degrades with decreasing filter bandwidth. In all cases, the simulated SNR increased above the prediction with decreasing bandwidth. The largest mean difference observed is 17 dB, for a normalized filter bandwidth of 0.01. This increase in energy over

the uncorrelated value is termed coherent SNR gain. It appears the correlation between the continuous scattering components adds coherent energy to the reflected signal, more like a deterministic spread component.

This effect is also observed with the composite scatterer comparison. However, the large point scatterer returns can swamp out the coherent energy, except for very small filter bandwidths. For mildly correlated scatterer the prediction and simulation disagree prior to the first highlight return, but the energy in the point scatterer returns is large, and beyond $T/T_s = 3.5$, the simulation and prediction agree quite well. With very correlated scattering, the coherent energy dominants, and the point scatterer returns are barely noticeable for all values of T/T_s. In general, a filter bandwidth of 0.05 or less was necessary for the coherent scatter to dominate, using a point scattering to continuous scattering strength ratio of 100.

6.2 Recommendations for Further Study

The encouraging results of this thesis imply the ambiguity function, scattering function approach can be applied to a wide variety of scatterers and receiver waveforms. This is not a new conclusion or result, rather a further demonstration of fact. The simulation results and predictions used in this thesis in particular suggest further efforts in two areas.

The first area is to increase the complexity of the scattering model. Straightforward modifications might include a time varying continuous scattering amplitude, several point scatters with random locations. The prediction equation can be similarly modified, subject to the restriction that the modification can be expressed analytically, in either a deterministic or statistical sense. Adding Doppler spreading is also possible in the model, but more difficult to include in the analytic prediction.

The other set of potential modifications to the model included an investigation of the effects of various processing waveforms. This is a simple change in the model, but requires a reworking of the prediction equation to include the new crossambiguity function. The value of this type of modification allows evaluation of very complex waveforms with a simple, well-behaved, scatterer.

ANNOTATED BIBLIOGRAPHY

[1] D.W. Ricker, personal communication, May 1983.

[2] H.L. VanTrees, Detection, Estimation and Modulation Theory (Part III). New York: John Wiley and Sons, 1971, chapter 9.

[3] Ibid., chapter 12.

[4] C.E. Cook and M. Bernfeld, Radar Signals, An Introduction to Theory and Application. New York: Academic Press, 1967, p. 9.

[5] VanTrees, chapters 9 and 12.

[6] R.S. Kennedy, Fading Dispersive Communications Channels. New York: Wiley-Interscience, 1969, p. 9.

[7] L.J. Ziomek, "A Scattering Function Approach to Underwater Acoustic Detection and Signal Design," Ph.D Thesis, The Pennsylvania State University, 1981, p. 53.

[8] VanTrees, chapter 12.

[9] Kennedy, p. 13.

[10] VanTrees, P. 415.

[11] Kennedy, p. 13.

[12] VanTrees, p. 416.

[13] Ibid.

[14] Ibid., p. 245.

[15] Cook and Bernfeld, p. 67.

[16] VanTrees, chapter 12.

[17] Ibid., chapter 9.

[18] Ziomek, p. 45.

[19] A. Papoulis, Probability, Random Variables, and Stochastic Processes. New York: McGraw-Hill, 1965, p. 370.

[20] S.A. Tretter, Introduction to Discrete-Time Signal Processing. New York: John Wiley and Sons, 1976, p. 235-241.

[21] IMSL (part 4), p. RLFOTH-1 and RLDOPH-1.

[22] VanTrees, p. 279.

[23] Digital Equipment Corp., VAX-11 Fortran Language Reference Manual. Maynard, Massachusetts: 1982. p. C-28.

[24] IMSL, IMSL Reference Manual (Part 2), Edition 9. Houston, Texas: 1982, p. GGNML-1.

[25] J.S. Bendat and A.G. Piersol, Random Data: Analysis and Measurement Procedures. New York: Wiley-Interscience, 1971, p. 119-122.

[26] Ibid., p. 67.

[27] W.B. Davenport and W.L. Root, An Introduction to the Theory of Random Signals and Noise. New York: McGraw-Hill, 1958. p. 31-32.

[28] A. Nuttall, personal communication, March, 1985.

[29] I.S. Gradshteyn and I.M. Ryzhik, Tables of Integrals, Series, and Products. New York: Academic Press, 1980, p. 285.

[30] M.R. Spiegel, Mathematical Handbook of Formulas and Tables, Schaum's Outline Series. New York: McGraw-Hill, 1968, p. 103.

[31] M. Abramowitz and I. Stegun, Handbook of Mathematical Functions with Formulas, Graphs, and Mathematical Tables. New York: Dover, 1965, p. 946.

APPENDIX A

DERIVATION OF THE CROSSAMBIGUITY FUNCTION

The general ambiguity function is defined as

$$A(\tau', \omega') = \left| \int_{-\infty}^{\infty} \tilde{f}(z-\frac{\tau'}{2}) \tilde{f}^*(z+\frac{\tau'}{2}) e^{j\omega' z} \, dz \right|^2 \qquad \text{(A-1)}$$

where

$$z = t - \tau + \frac{\tau'}{2}$$

$$\tau' = \tau - \tau_0$$

$$\omega' = \omega - \omega_0 ,$$

where τ_0 and ω_0 are the delay and doppler of the actual scattering function and τ and ω are the delay and Doppler assumed by the receiver.

$A(\tau',\omega')$ is a measure of the mean square deviation of the transmit waveform with a delayed and shifted version of itself [22]. The function $A(\tau',\omega')$ is referred to as the autoambiguity function of the signal f(t). This result may be extended to two different waveforms. The crossambiguity function of f(t) and g(t) is then defined as,

$$\left| X(\tau',\omega') \right|^2 = \left| \int_{-\infty}^{\infty} f(z-\frac{\tau'}{2}) \, \tilde{g}^*(z+\frac{\tau'}{2}) e^{j\omega' z} dz \right|^2 \qquad \text{(A-2)}$$

and is a measure of the mean square error of one signal, in our case the transmit signal, with a delayed and shifted version a second signal, referred to as the receiver processing signal.

$\tilde{f}(t)$ and $\tilde{g}(t)$ are assumed to be of the form,

$$\tilde{f}(t) = \frac{1}{\sqrt{T_s}} \, , \; \frac{T_s}{2} < t < \frac{T_s}{2} \tag{A-3}$$

$$\tilde{g}(t) = \frac{1}{\sqrt{T}} \, , \; \frac{-T}{2} < t < \frac{T}{2} \, , \tag{A-4}$$

where $T > T_s$.

Equations 3 and 4 imply the envelope of the transmit signal is assumed to fall completely within the duration of the processing signal and $T_s \leq T$. Substitution of these signals into Equation A-2 yields

$$\left| \chi(\tau', \omega') \right|^2 = \left| \int_{-\frac{T_s}{2}}^{\frac{T_s}{2}} \frac{1}{\sqrt{T \cdot T_s}} e^{j\omega' t} \, dt \right|^2 \tag{A-5}$$

$$= \left| \frac{1}{\sqrt{T \cdot T_s}} \; \frac{e^{j\omega' \frac{T_s}{2}} - e^{-j\omega' \frac{T_s}{2}}}{j\omega'} \right|^2 \tag{A-6}$$

$$= \left| \frac{1}{\sqrt{T \cdot T_s}} \; \frac{2}{\omega'} \; \sin\left(\frac{\omega' T_s}{2}\right) \right|^2 \tag{A-7}$$

Defining sinc(x) as sin(x)/x, and multiplying Equation A-7 by $2T_s/2T_s$ yields

$$\left|X(\tau',\omega')\right|^2 = \left|\frac{1}{\sqrt{T \cdot T_s}}\ T_s\ \mathrm{sinc}\left(\frac{\omega' T_s}{2}\right)\right|^2 \qquad \text{(A-8)}$$

$$= \frac{T_s}{T}\ \mathrm{sinc}^2\left(\frac{\omega' T_s}{2}\right) \qquad \text{(A-9)}$$

APPENDIX B

GENERATION OF RANDOM NUMBERS

B.1 Generation of Uniform Random Numbers

The target scattering simulation uses the operating system supplied uniform random number generator, RAN, to compute uniform numbers in the range [0,1] [23]. The first call to the generator requires a unique integer seed, which should also be large and odd. This seed initializes the generator, and is calculated by doubling the value of the computer system time clock, in seconds, and adding one. Twenty additional calls are then made to RAN, to produce the first seed value used for the scattering simulation. Since the simulation data was computed over a number of days, none of the original seeds were identical, and it is reasonable to assume the sequences of random numbers generated used in the simulation are statistically independent from each other.

B.2 Generation of Gaussian Numbers

Each individual scatterer is modeled as a sample function from a complex Gaussian process. To generate these scatterers in simulation, two real, independent Gaussian numbers are required. Each pair of numbers is obtained by successive calls to the Gaussian number Generator GGNML, a subroutine in the IMSL Mathematical Library [24]. The generator output was tested for two statistical properties;

distribution of generator outputs, and correlation between sequences generated with different initialization seeds.

Figures 39 and 40 are histogram plots for GGNML outputs for 100 and 1000 sample sets, respectively. While the theoretical values of the mean and standard deviation are 0 and 1, the histogram of the 100 sample set, Figure 3 has a mean of 0.04 and a standard deviation of 0.92. A chi-squared test was performed on this set, and the assumption of Gaussian distribution was satisfied with 80 percent confidence [25]. For the 1000 sample set, the mean and standard deviation are 0.01 and 1.01, very close to the values of the continuous distribution. The confidence that this sequence is Gaussian distributed is greater than 95 percent. For sets of greater than 10000 samples, the mean and standard deviation are equal to the continuous distribution values, and on the basis of these tests, it is concluded that the random number generator GGNML does produce sequences of numbers that are Gaussian distributed.

The second test applied to these sequences gives a measure of the independence between samples generated with different initial seed values. Figure 41 is a representative plot of the autocorrelation of a 1024 sample set. The ordinate of the plot is correlation magnitude, normalized between -1 and 1. The abscicca is delay, in units of samples. The correlation magnitude is less than 0.1, beyond 10 samples of delay. This indicates that the sequence is poorly

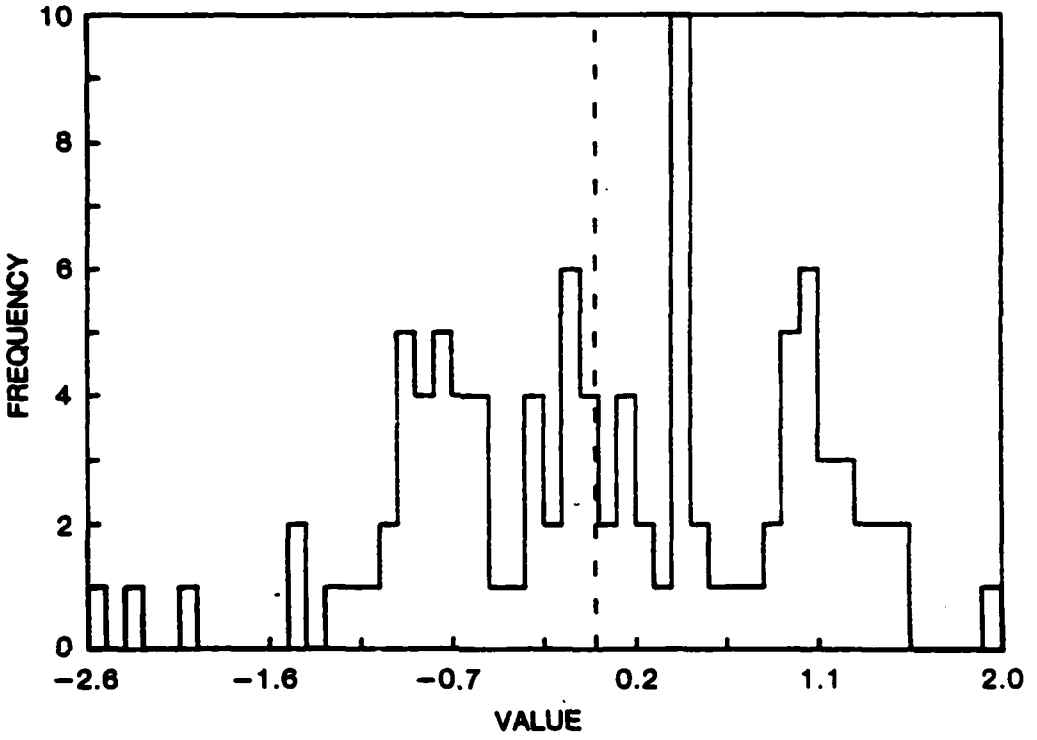

FIGURE 39. Histogram of random number generator for a sample set size of 100. Distribution mean = 0.04, and standard deviation = 0.92.

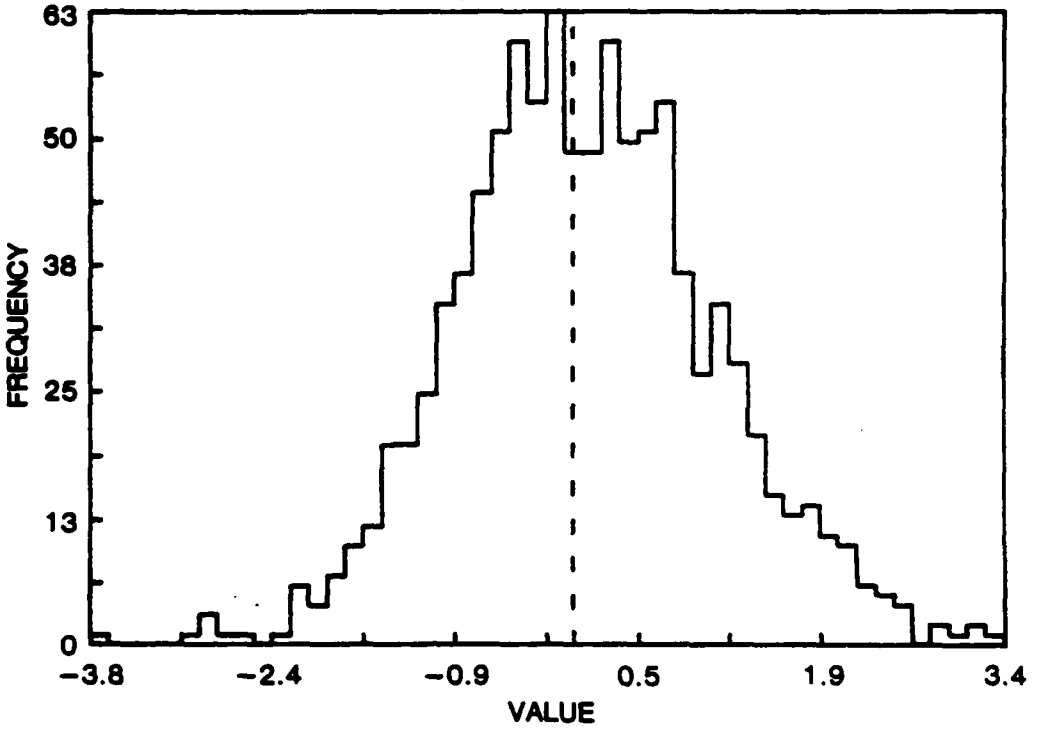

FIGURE 40. Histogram of random number generator for a sample set size of 1000. Distribution mean = 0.01, and standard deviation = 1.01.

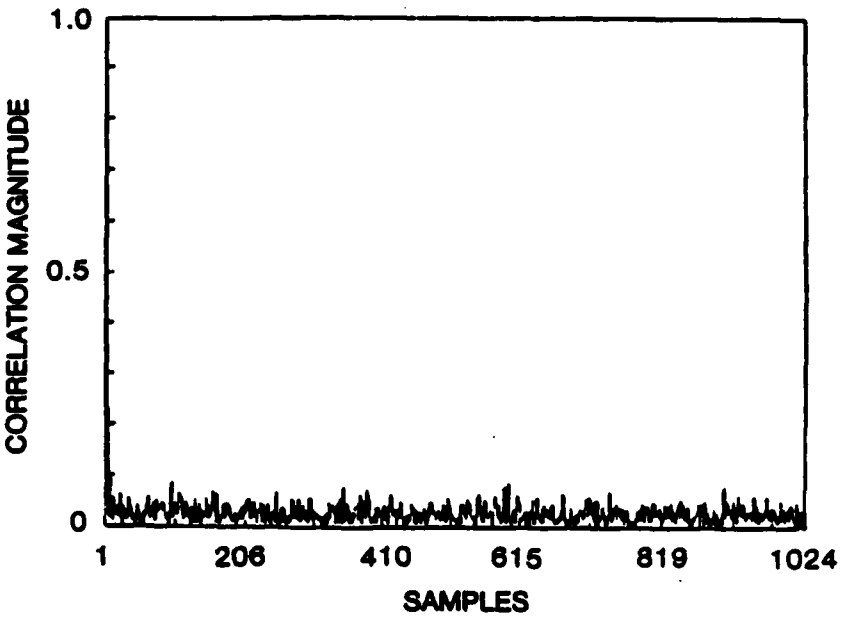

FIGURE 41. Autocorrelation of random number generator output for a sample set size of 1024.

correlated with itself, a indication that successive generator outputs are uncorrelated.

A representative crosscorrelation between two sequences generated with different initial seed values is shown in Figure 42. Unlike the autocorrelation example, where the correlation magnitude at a delay of zero samples is unity, the crosscorrelation magnitude is low across all delay. These results indicate that the Gaussian number generator outputs are reasonably uncorrelated with each other. This result is expected, since the theoretical distribution values are defined to be statistically independent [26]. While statistical independence of the generator output cannot be inferred on the basis of correlation, that the outputs show poor correlation, both auto and cross, is sufficient for this thesis to validate the random number generator output [27].

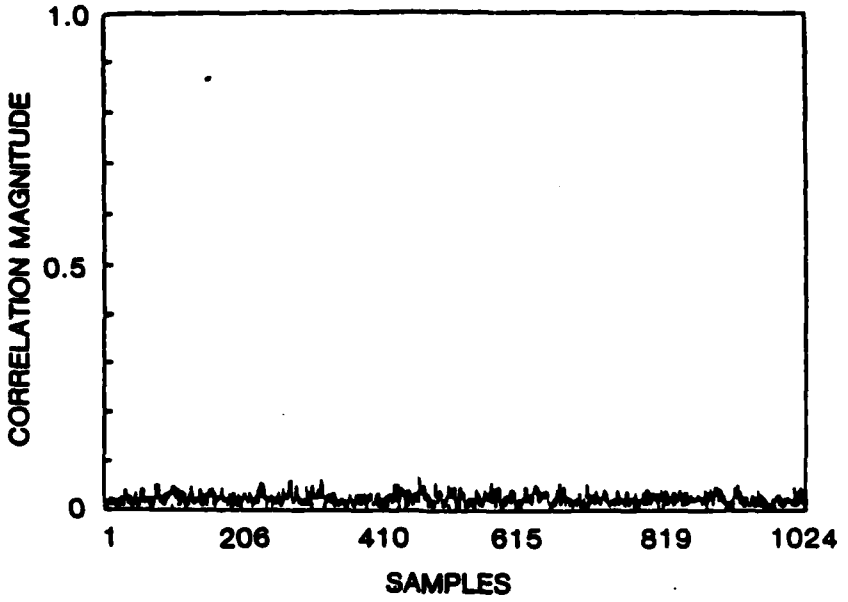

FIGURE 42. Crosscorrelation of random number generator output for a sample set size of 1024.

APPENDIX C

CALCULATION OF VARIANCE OF SIGNAL-TO-NOISE RATIO

The signal-to-noise ratio is computed by evaluating

$$SNR = \frac{\frac{1}{N}\sum_{k=1}^{N}|S_k|^2}{\frac{1}{N}\sum_{k=1}^{N}|N_k|^2} \qquad (C\text{-}1)$$

$$= \frac{\sum_{k=1}^{N}|S_k|^2}{\sum_{k=1}^{N}|N_k|^2} \qquad (C\text{-}2)$$

and

$$S_k = S_{k_R} + j\ S_{k_I} \qquad (C\text{-}3)$$

where S_{k_R} and S_{k_I} are zero mean Gaussian variables. Therefore S_k is with 2 degrees of freedom. Similarly, N_k is X^2 with 2 degrees of freedom. The sum of N chi-squared variables is also chi-squared, with 2N degrees of freedom.

From Nuttall [28], the PDF of gamma variates is

$$p_x(u) = \frac{\alpha^{\mu} u^{\mu-1} \exp(-\alpha u)}{\Gamma(u)} \tag{C-4}$$

$$p_y(u) = \frac{\beta^{\nu} u^{\nu-1} \exp(-\beta u)}{\Gamma(u)} \tag{C-5}$$

and the PDF of the ratio $z = x/y$ for x and y independent is

$$p_z(u) = \frac{\Gamma(\mu+\nu)}{\Gamma(\mu)\Gamma(\nu)} \frac{r(ru)^{\mu-1}}{(1+ru)^{\nu+\mu}} \tag{C-6}$$

where

$$r = \frac{\sigma_y^2}{\sigma_x^2} \tag{C-7}$$

For the case of interest $\mu = \nu = N$, an integer. Equation 6 may be reduced to,

$$p_z(u) = \frac{(2N-1)!}{(N-1)!^2} \cdot \frac{r(ru)^{N-1}}{(1+ru)^{2N}} . \tag{C-8}$$

The Θ^{th} moment is computed by,

$$\int_{-\infty}^{\infty} u^{\Theta} p_z(u) du = \int_{-\infty}^{\infty} \frac{(2N-1)!}{(N-1)!^2} \frac{u^{\Theta} r(ru)^{N-1}}{(1+ru)^{2N}} . \tag{C-9}$$

From Gradshteyn and Ryzhik [29],

$$\int_{-\infty}^{\infty} \frac{x^{\nu-1}}{(1+\beta x)^{\mu}} dx = \beta^{-\mu} B(\mu, \nu-\mu) \tag{C-10}$$

where B(x,y) is the Beta function. The conditions for existence of solution are $|\beta| < \pi$ and $v > \mu > 0$. Substituting for μ and v in Equation B-10 gives,

$$u^{\Theta} = \frac{(2N-1)!}{(N-1)!^2} r^{-\Theta} B(N+\Theta, N-\Theta) . \qquad (C-11)$$

where the conditions on the solution $N > \Theta$, $N > 1$, $r < |\pi|$, all of which are satisfied. The Beta function is reduced to the ratio of Gamma functions by the relation [30],

$$B(x,y) = \frac{\Gamma(x)\Gamma(y)}{\Gamma(x+y)} , \qquad (C-12)$$

and Equation 11 is written as

$$u^{\Theta} = \frac{(2N-1)!}{(N-1)!^2} \cdot \frac{(N+\Theta+1)!\,(N-\Theta-1)!}{(2N-1)!\, r^{\Theta}} \qquad (C-13)$$

The first moment, $\Theta = 1$, is,

$$u^{(1)} = \frac{N}{N-1} \frac{\sigma_x^2}{\sigma_y^2} . \qquad (C-14)$$

The second moment, $\Theta = 2$, is,

$$u^{(2)} = \frac{N(N+1)}{(N-1)(N-y)} \left(\frac{\sigma_x^2}{\sigma_y^2} \right)^2 . \qquad (C-15)$$

and the variance,

$$\sigma_z^2 = \frac{N(N+1)}{(N-1)(N-2)r^2} - \frac{N^2}{(N-1)^2 r^2} \qquad \text{(C-16)}$$

$$= \frac{N}{(N-1)r^2} \cdot \left[\frac{2N-1}{(N-1)(N-2)}\right] \qquad \text{(C-17)}$$

Equation C-17 is identical in form to the variance of the F distribution with 2N degrees of freedom [31]. It is therefore concluded that variance of the simulated signal-to-noise, normalized by the ratio of the noise variance to signal variance is F distributed. Confidence limits may now be computed by calculating F(2N,2N) for a specific α.

INITIAL DISTRIBUTION LIST

Addressee		No. of Copies
NAVSEA	(63D, CDR G. Graham)	1
NRL	(Code 5120, L. B. Palmer; 5160, R. Doolittle; Library)	3
NORDA	(Code 113, B. Adams, R. Farwell; Library)	3
NCSC	(L. Satkowiak)	1
NOSC	(Code 732, Dr. C. Persons)	1
ARL/PSU	(C. Ackerman, D. Ricker, A. Stuart, F. Menotti, D. Thompson, W. Zierke, J. Shive)	7
DIA		1
DTIC		2
DREP	(Dr. Thomson)	1

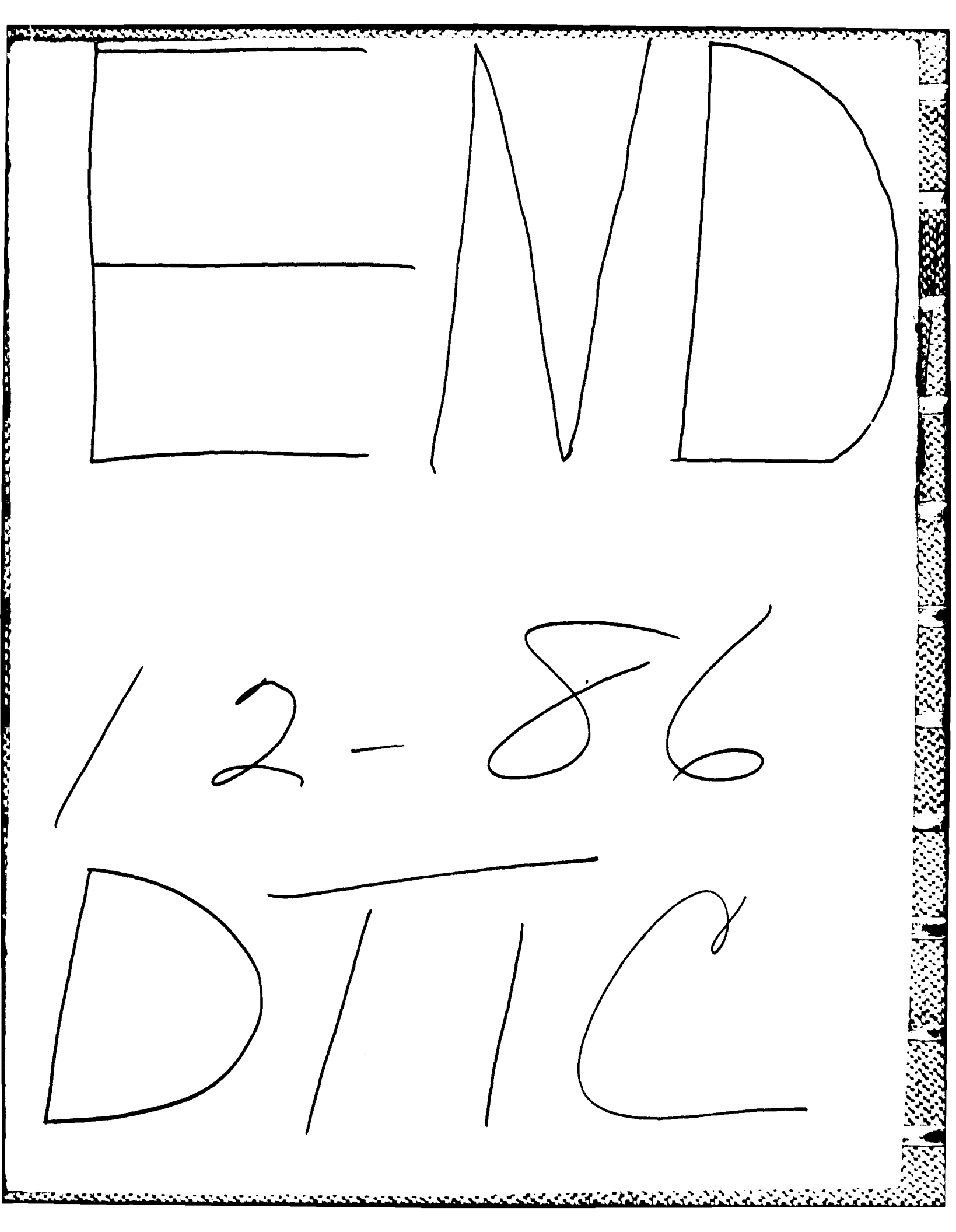
END
12-86
DTIC